Article

Functional gene delivery to and across brain vasculature of systemic AAVs with endothelial-specific tropism in rodents and broad tropism in primates

Xinhong Chen [1], Damien A. Wolfe[1], Dhanesh Sivadasan Bindu[2], Mengying Zhang[1], Naz Taskin[3], David Goertsen [1], Timothy F. Shay [1], Erin E. Sullivan [1], Sheng-Fu Huang[4], Sripriya Ravindra Kumar [1], Cynthia M. Arokiaraj [1], Viktor M. Plattner [5], Lillian J. Campos [6], John K. Mich[3], Deja Monet[3], Victoria Ngo[7], Xiaozhe Ding [1], Victoria Omstead[3], Natalie Weed[3], Yeme Bishaw[3], Bryan B. Gore [3], Ed S. Lein [3], Athena Akrami [5], Cory Miller[7], Boaz P. Levi [3], Annika Keller [4,8], Jonathan T. Ting[3,9], Andrew S. Fox [6], Cagla Eroglu [2] & Viviana Gradinaru [1]✉

Delivering genes to and across the brain vasculature efficiently and specifically across species remains a critical challenge for addressing neurological diseases. We have evolved adeno-associated virus (AAV9) capsids into vectors that transduce brain endothelial cells specifically and efficiently following systemic administration in wild-type mice with diverse genetic backgrounds, and in rats. These AAVs also exhibit superior transduction of the CNS across non-human primates (marmosets and rhesus macaques), and in ex vivo human brain slices, although the endothelial tropism is not conserved across species. The capsid modifications translate from AAV9 to other serotypes such as AAV1 and AAV-DJ, enabling serotype switching for sequential AAV administration in mice. We demonstrate that the endothelial-specific mouse capsids can be used to genetically engineer the blood-brain barrier by transforming the mouse brain vasculature into a functional biofactory. We apply this approach to Hevin knockout mice, where AAV-X1-mediated ectopic expression of the synaptogenic protein Sparcl1/Hevin in brain endothelial cells rescued synaptic deficits.

Malfunction of cell types comprising vasculature within the brain, including endothelial cells, can facilitate the progression of neurological disorders[1-4]. However, the study of vasculature is hampered by limited options for versatile, cell-type-specific transgene delivery. Adeno-associated virus (AAV) vectors offer promise for gene delivery to the brain, but are commonly administered via intracranial injections, resulting in tissue damage and limited and uneven spatial coverage[5,6]. Systemic AAV delivery provides a non-invasive, brain-wide alternative[7-11], but specifically targeting cell types of interest remains a challenge.

Having previously engineered vectors that efficiently cross the blood-brain barrier (BBB) with broad tropism in rodents (e.g., AAV-PHP.eB)[7,12-14], we recently turned our focus to identify vectors with cell-type biased tropism. From the PHP.B sequence family, we identified PHP.V1, which, when intravenously delivered, has enhanced potency for endothelial cells, although it also transduces astrocytes and

neurons[13]. While an improvement, PHP.V1 still requires cell type-specific promoters whose large size limits the choice of transgenes and it only works in certain mouse strains. In addition, capsid entry into other cell types may induce an immune response, creating a confounding effect. Similar problems also apply to the previously-reported BR1 endothelial variant; BR1 transduces a large number of neurons and astrocytes besides endothelial cells[15,16]. With the increasing number of engineered AAVs reported, there are also increasing examples showing their potentially distinct tropism across species[10,11], emphasizing the necessity for the testing of engineered variants in different species, especially non-human primates (NHPs).

Another challenge remaining for AAV gene delivery is successful re-administration, which may be needed to maximize therapeutic effect, particularly given occasional loss of transgene expression over time reported with AAV gene delivery[17]. While neutralizing antibodies induced by initial AAV administration can prevent sequential administration of the same AAV[18], switching to another AAV serotype with similar or complementary features is a potential solution[19,20] that remains underexplored.

An AAV with potent and specific tropism for brain vasculature would enable new strategies for gene therapy. As the leading platform for in vivo delivery of gene therapies, AAV vectors have been used to deliver diverse therapeutic genes to treat a broad spectrum of disorders[21,22], including those resulting from loss of either cell-autonomous factors or factors which act on neighboring cells regardless of genotype. For disorders caused by the loss of function of a single non-cell-autonomous factor, such as mucopolysaccharidosis[23], the factor is typically a secreted protein[21]. In these cases, gene therapy could target a healthy cell population, transforming those cells into a "biofactory" for the production and secretion of a therapeutic protein that could cross-correct affected cells. Currently, however, therapeutic proteins produced from peripheral biofactories, most commonly the liver, enter the CNS with low efficiency and fall short of rescuing phenotypes in CNS disorders[24,25]. Given its broad distribution and close proximity to other cell types within the CNS, AAV-transformed brain vasculature may serve as a better biofactory for the CNS.

Here, through a combination of directed evolution and semi-rational engineering, we identified a family of novel vectors, including AAV-X1 and AAV-X1.1, which target brain endothelial cells specifically and efficiently following systemic delivery in mice with a ubiquitous promoter. We characterized these novel AAVs across rodent models (genetically diverse mouse strains and rats), non-human primates (marmosets and rhesus macaques), and ex vivo human brain slices, demonstrating brain endothelial-specific cell targeting in rodents and broad CNS targeting in primates. To illustrate the utility of AAV-X1 for CNS delivery of neuroactive proteins, we transformed mouse brain endothelial cells into a biofactory for producing the synaptogenic protein Sparc-like protein 1 (Sparcl1)/Hevin. Hevin/Sparcl1 is an astrocyte-secreted protein that controls the formation of vesicular glutamate transporter 2 (VGluT2)-containing synapses such as thalamocortical synapses[26–28]. AAV-X1-mediated ectopic expression of Sparcl1/Hevin in brain endothelial cells was sufficient to rescue the thalamocortical synaptic loss phenotype of Sparcl1/Hevin knockout mice. We also demonstrate the transferability of AAV-X1's properties from the AAV9 serotype to AAV1, enabling repeated AAV administration to increase CNS transduction. In summary, we provide novel engineered systemic AAVs for brain endothelial-specific cell targeting in rodents and broad CNS targeting from rodent to primate with the potential for re-administration.

Results
A novel AAV capsid specifically targets brain endothelial cells in mice following systemic administration
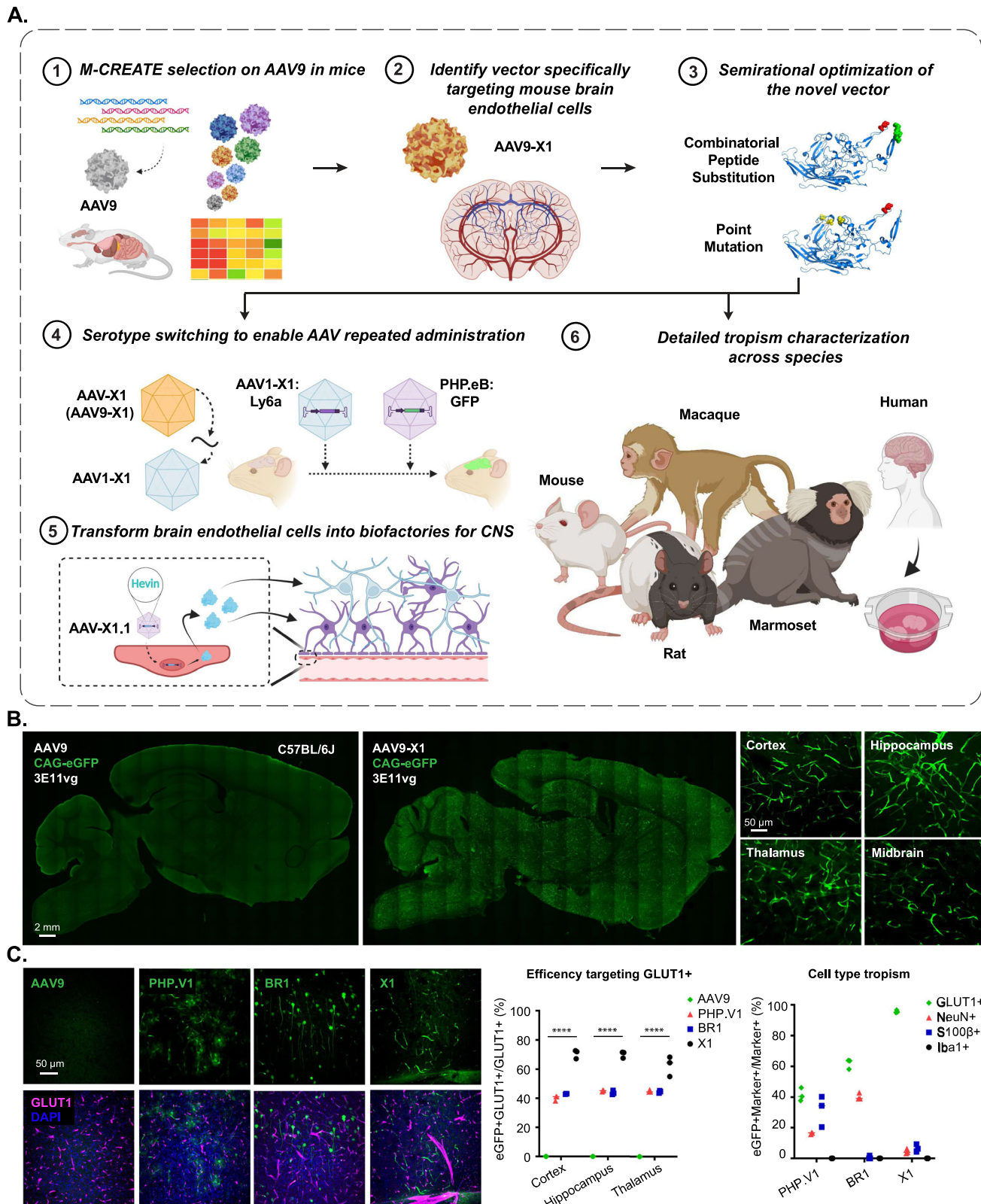As a starting point for engineering, we chose AAV9, which targets the CNS with low efficiency following systemic delivery. We inserted randomized 7-mer peptides between positions 588 and 589 of AAV9 and injected the resulting virus library intravenously into transgenic mice expressing Cre from either the Tek (targeting endothelial cells) or Synapsin I (Syn, targeting neuronal cells) promoter. After 2 rounds of M-CREATE selection[13], we identified a variant, named AAV-X1, which was among the most enriched in Tek-Cre mice, indicating potential endothelial tropism in mice (Fig. 1A). To characterize the transduction profile of AAV-X1 in vivo we packaged it with a single-stranded (ss) AAV genome carrying a strong ubiquitous promoter, CAG, driving the expression of an eGFP reporter. Three weeks after IV administration to C57BL/6 J mice, we observed specific and efficient targeting of the vasculature across brain regions (Fig. 1B). To compare the vascular targeting of AAV-X1 to that of previously engineered capsids, we repeated the experiment along with AAV9, AAV-PHP.V1, and AAV-BR1[13,15]. After 3 weeks of expression, AAV-X1 exhibited higher efficiency and higher specificity in targeting brain endothelial cells compared to all three controls (Fig. 1C). At a dose of 3×10^{11} viral genomes (vg) per mouse, AAV-X1 transduced ~65–70% of GLUT1+ (endothelial marker) cells across the cortex, hippocampus, and thalamus. In comparison, AAV-PHP.V1 and AAV-BR1 transduced ~40% of GLUT1+ cells, while AAV9 transduced ~1% of the endothelial cells. AAV-X1 also exhibited superior specificity towards vasculature; ~95% of the cells transduced by AAV-X1 were GLUT1+. In contrast, AAV-BR1 and AAV-PHP.V1 transduced GLUT1+ cells with much less specificity, with only 60% and 40% of transduced cells being GLUT1+, respectively. AAV-BR1 also targeted neurons, while AAV-PHP.V1 also targeted neurons and astrocytes (Fig. 1C). Further staining with CD31 or Podocalyxin (endothelial cells), Calponin 1 (smooth muscle cells), CD206 (perivascular macrophages), GFAP (astrocytes) and CD13 (pericytes) confirmed the high efficiency and specificity of AAV-X1 in targeting brain endothelial cells (Supplementary Fig. 1A–D). Interestingly, the endothelial cells in the choroid plexus (CP) were not transduced by AAV-X1 (Supplementary Fig. 1C). In summary, the novel vector AAV-X1 not only exhibits significant improvement in targeting the CNS compared to its parent AAV9 but also shows high specificity towards brain endothelial cells.

Semi-rational refinement of X1's peripheral tropism by further engineering cargo and capsid
While the novel variant X1 exhibited significant improvement in transducing the CNS endothelium compared to AAV9, it maintained a similar level of liver transduction. Therefore, we next explored strategies to further refine the vector's tropism, either by incorporating specific cargo elements or by further engineering the capsid (Fig. 2A).

We first explored whether adding a regulatory element to X1's cargo could reduce liver expression. When incorporated into the genome, microRNA target sites induce microRNA-mediated post-transcriptional transgene silencing[29]. MicroRNA-122 (miR122) is highly specific to the liver[30] and incorporation of its target site has been shown to reduce AAV expression in the liver[31]. We cloned three copies of miR122's target site (TS) into a CAG-eGFP genome and packaged it in the X1 vector. Three weeks after IV delivery of X1: CAG-eGFP-miR122TS, we observed a large reduction in liver expression, indicating that future applications of X1 could incorporate miR122 TS for liver detargeting (Fig. 2B, bottom left panel).

While cargo engineering reduced transgene expression in the liver, the AAV capsid still entered the liver and might trigger an immune response. Therefore, we next explored whether further engineering of the X1 capsid could achieve similar liver detargeting, and potentially further boost CNS transduction. Structural information[32] and previous engineering efforts[14] suggest that the 455 loop of AAV9 potentially interacts with the 588 loop and affects receptor binding. A 7-mer substitution of 452–458 of PHP.eB was found to further boost that capsid's CNS targeting ability and enable potent transduction of the mouse and marmoset CNS while detargeting the AAV from the liver[14]. Therefore, we took three 7-mer

A.

1. *M-CREATE selection on AAV9 in mice*

AAV9

2. *Identify vector specifically targeting mouse brain endothelial cells*

AAV9-X1

3. *Semirational optimization of the novel vector*

Combinatorial Peptide Substitution

Point Mutation

4. *Serotype switching to enable AAV repeated administration*

AAV-X1 (AAV9-X1)

AAV1-X1

AAV1-X1: Ly6a

PHP.eB: GFP

6. *Detailed tropism characterization across species*

Mouse · Macaque · Human · Marmoset · Rat

5. *Transform brain endothelial cells into biofactories for CNS*

Hevin

AAV-X1.1

B.

AAV9 · C57BL/6J · CAG-eGFP · 3E11vg

AAV9-X1 · CAG-eGFP · 3E11vg

Cortex · Hippocampus · Thalamus · Midbrain

50 µm · 2 mm

C.

AAV9 · PHP.V1 · BR1 · X1

50 µm

GLUT1 · DAPI

Efficency targeting GLUT1+

eGFP+GLUT1+/GLUT1+ (%)

AAV9 · PHP.V1 · BR1 · X1

Cortex · Hippocampus · Thalamus

Cell type tropism

eGFP+Marker+/Marker+ (%)

GLUT1+ · NeuN+ · S100β+ · Iba1+

PHP.V1 · BR1 · X1

peptides identified from that PHP.eB 455 loop selection and substituted them into X1, creating X1.1, X1.2, and X1.3. Compared to X1, X1.1 showed further improvement in targeting the CNS, transducing ~82–85% of GLUT1+ cells across brain regions (Fig. 2B, C). X1.1 also maintained high specificity in targeting the brain vasculature; ~90-92% of transduced cells were GLUT1+ (Fig. 2C, right). X1.1 showed a similar expression pattern as X1 and AAV9 in peripheral organs and neither

was vasculature-tropic in peripheral organs (Supplementary Fig. 2A, B). To fully capture X1.1's performance across organs, we measured vector genomes and RNA transcripts following systemic administration in mice. We observed increased presence in CNS and reduced targeting of some peripheral organs compared to AAV9, especially in RNA transcript levels. In some organs, such as the heart, higher DNA but lower RNA levels suggest possible non-specific vascular uptake, which

Fig. 1 | Engineered AAVs can specifically target the brain endothelial cells in mouse following systemic delivery. A An overview of the engineering and characterization of the novel capsids. (1): Evolution of AAV9 using Multiplexed-CREATE and (2): identification of a novel vector, AAV-X1, that transduces brain endothelial cells specifically and efficiently following systemic administration in mice. (3): Combinatorial peptide substitution and point mutation to further refine the novel vector's tropism, yielding improved vectors. (4): Transferring the X1 peptide to the AAV1 backbone to enable serotype switching for sequential AAV administration. (5): Utilizing AAV-X1 to transform the brain endothelial cells into a biofactory, producing Hevin for the CNS. (6): Validation of the novel AAVs across rodent models (genetically diverse mice strains and rats), NHPs (marmosets and macaques), and ex vivo human brain slices. Created with BioRender.com. **B** (Left) Representative images of AAV (AAV9, AAV-X1) vector-mediated expression of eGFP (green) in the brain (scale bar: 2 mm). (Right) Zoomed-in images of AAV-X1-mediated expression of eGFP (green) across brain regions, including the cortex, hippocampus, thalamus,

and midbrain (scale bar: 50 µm). (C57BL/6J, $n = 3$ per group, 3E11 vg IV dose per mouse, 3 weeks of expression). **C** (Left) Representative images of AAV (AAV9, PHP.V1, BR1, and AAV-X1) vector-mediated expression of eGFP (green) in the cortex. Tissues were co-stained with GLUT1 (magenta) (scale bar: 50 µm). (Middle) Percentage of AAV-mediated eGFP-expressing cells that overlap with the GLUT1+ marker across brain regions, representing the efficiency of the vectors' targeting of GLUT1+ cells. A two-way ANOVA and Tukey's multiple comparisons tests with adjusted P values are reported (****$P < 0.0001$. $P = 1.8e-15$ for AAV9 versus X1.1 in the cortex. $P = 1.8e-15$ for AAV9 versus X1.1 in the hippocampus. $P = 1.8e-15$ for AAV9 versus X1.1 in the thalamus). Each data point shows the mean of three slices per mouse. (Right) Percentage of GLUT1+, NeuN+, S100β+ and Iba1+ markers in AAV-mediated eGFP-expressing cells across brain regions, representing the specificity of the vectors' targeting of GLUT1+ cells. (C57BL/6J, $n = 3$ per group, 3E11 vg IV dose per mouse, 3 weeks of expression). Source data are provided as a Source Data file.

requires further investigation (Supplementary Fig. 2C–F). Some applications in mice require a higher dose of AAVs; therefore, we injected X1.1 at higher doses and verified that it maintained its high specificity against brain endothelial cells (Supplementary Fig. 2G, H). X1.1 was capable of packaging viral genomes with similar efficiency to AAV9 (Fig. 2D). Given X1.1's high efficiency transduction of brain endothelial cells, we performed a dye perfusion experiment to evaluate whether AAV transduction may compromise BBB integrity. We did not detect increased leakage in the BBB compared to uninjected mice (Supplementary Fig. 3A).

Having seen that X1 can accommodate additional capsid changes, we next investigated whether we could optimize the vector's tropism by mutating sites known to mediate receptor interactions and affect tropism. N272 and W503 have been shown to be required for AAV9's binding to galactose[33–36], and mutation of W503 has been shown to reduce the liver transduction of AAV9[33]. Therefore, we decided to mutate N272 or W503 of X1 to alanine, yielding X1.4 and X1.5, respectively. S386 of AAV9 and Q386 of AAV1 have also been shown to mediate receptor interaction[36,37], so we mutated S386 of X1 to alanine, yielding X1.6. Following IV delivery of these vectors in mice, we observed that X1.4 and X1.5 showed reduced liver transduction while maintaining their brain-endothelial tropism (Fig. 2B, bottom).

To explore the novel vectors' potential for application in different physiological contexts, we tested the X1.1 vector in young (2.5 months old) versus aged (2.5 years old) mice and did not observe an obvious difference in CNS transduction after 3 weeks' expression. We also did not observe an obvious sex difference in its CNS tropism (Supplementary Fig. 3B).

X1 vectors transduce brain endothelial cells across diverse mouse strains and rats in a Ly6a-independent manner

The previously-engineered AAV-PHP.eB has been shown to rely on improved binding to Ly6a for its increased CNS tropism[38–40], and polymorphism of Ly6a across mouse strains contributes to its strain-specific phenotype[38,39]. Therefore, we explored whether the improved CNS targeting of X1 and its further-engineered versions is also dependent on Ly6a binding. We observed that transient over-expression of Ly6a in HEK cells boosted PHP.eB transduction but had no significant effect on X1 transduction (Supplementary Fig. 3C). Surface plasmon resonance (SPR) experiments designed to amplify even weak interactions with Ly6a showed that while both PHP.eB and PHP.V1 exhibited strong binding to Ly6a, explaining the strain-specific phenotype of PHP.V1 (Fig. 3A)[13], neither X1 nor X1.1 bound Ly6a (Fig. 3A). These results suggest that X1 and its derivatives utilize a novel mechanism of cell targeting.

The Ly6a-independence of the X1 vectors prompted us to test their translatability across mice strains. Systemic delivery of X1 capsid packaged with ssAAV:CAG-eGFP in BALB/cJ, CBA/J, and FVB/NJ mouse strains resulted in efficient transduction of endothelial cells across

brain regions (Fig. 3B, C). Interestingly, though, we observed differential expression patterns in the liver across the strains, with minimal liver transduction in BALB/cJ and CBA/J strains (Fig. 3C).

We next investigated the new variants' transduction profile in rats. Following intravenous delivery of X1.1 capsid packaging ssAAV:CAG-tdTomato in adult Lister Hooded rats, we observed robust expression in the brain (Fig. 3D). X1.1-induced expression overlapped with GLUT1+, indicating that its tropism towards endothelial cells is conserved (Fig. 3E).
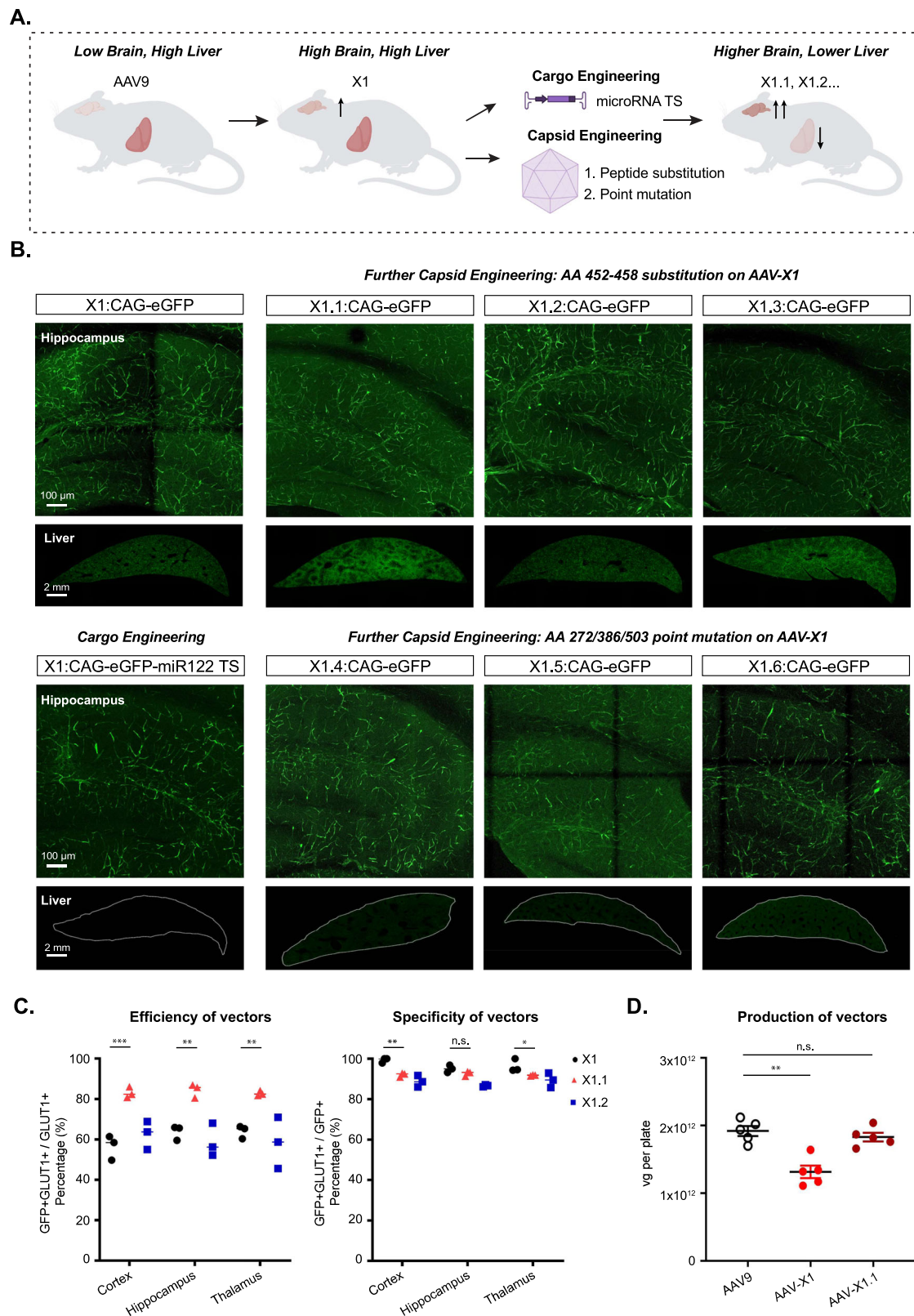
To explore tropism when the BBB is not intact, we next tested the vectors in pericyte-deficient mice (Supplementary Fig. 3D)[41,42]. We observed increased transduction of other cell types compared to control mice (Supplementary Fig. 3E). Interestingly, astrocytes with end-feet on the brain vasculature were transduced in pericyte-deficient mice but not in control mice (Supplementary Fig. 3F), indicating that the novel vectors' specificity towards endothelial cells may be dependent on the status of the BBB.

Serotype switching of X1 from AAV9 into AAV1 enables repeated administration of AAV in mice

Repeated administration of AAV is desired for certain applications; however, neutralizing antibodies induced by an initial administration prevent the subsequent delivery of similar AAVs[20,43]. One potential solution is to switch AAV serotypes in sequential administrations, but most of the novel AAVs engineered to target the CNS, including PHP.B and AAV-X1, are based on AAV9. To overcome this potential hurdle and enable repeated administration, we sought to transfer the X1 peptide and recreate our engineered AAV in another natural serotype.

Mixed results have been reported for previous attempts to directly transfer the PHP.B or PHP.eB peptide to natural serotypes, usually AAV1, due to its CNS tropism[44–47]. We inserted the 7-mer peptide of PHP.B into the AAV1 capsid, creating the hybrid AAV1-PHP.B (Fig. 4B). Intravenous injection of adult mice with AAV1-PHP.B packaging CAG-eGFP showed no obvious improvement in brain transduction compared to AAV1. However, AAV1-X1, created by a similar strategy, showed robust CNS expression in a pattern similar to that of X1, efficiently and specifically targeting GLUT1+ endothelial cells (Fig. 4C). We also tested a similar strategy and inserted the X1 peptide in AAV-DJ, creating AAV-DJ-X1. Similar to AAV1-X1, AAV-DJ-X1 showed improved CNS targeting compared to AAV-DJ following systemic delivery (Supplementary Fig. 4A). These results indicate that X1's phenotype can be transferred to some other serotypes by transferring the 7-mer peptide, although this would need to be tested individually for each new serotype.

To test AAV1-X1's potential to enable repeated administration, we utilized the virus for Ly6a supplementation. Polymorphisms in Ly6a in certain mouse strains, such as CBA/J and BALB/cJ, greatly reduce the CNS permeability of PHP.eB[38–40]. The brain endothelial cell tropism of X1 and AAV1-X1 prompted us to utilize them to express C57BL/6J-like

A.

Low Brain, High Liver — AAV9

High Brain, High Liver — X1

Cargo Engineering — microRNA TS

Capsid Engineering
1. Peptide substitution
2. Point mutation

Higher Brain, Lower Liver — X1.1, X1.2...

B.

Further Capsid Engineering: AA 452-458 substitution on AAV-X1

X1:CAG-eGFP | X1.1:CAG-eGFP | X1.2:CAG-eGFP | X1.3:CAG-eGFP

Hippocampus (100 µm)
Liver (2 mm)

Cargo Engineering — X1:CAG-eGFP-miR122 TS

Further Capsid Engineering: AA 272/386/503 point mutation on AAV-X1

X1.4:CAG-eGFP | X1.5:CAG-eGFP | X1.6:CAG-eGFP

Hippocampus (100 µm)
Liver (2 mm)

C.

Efficiency of vectors — GFP+GLUT1+ / GLUT1+ Percentage (%) — Cortex, Hippocampus, Thalamus (*** , **, **)

Specificity of vectors — GFP+GLUT1+ / GFP+ Percentage (%) — Cortex, Hippocampus, Thalamus (**, n.s., *)

● X1 ▲ X1.1 ■ X1.2

D.

Production of vectors — vg per plate — AAV9, AAV-X1, AAV-X1.1 (**, n.s.)

Ly6a in the BBB of these non-permissive strains, and thereby increase the permeability of those animals' BBB for AAV9-based PHP.eB when it is subsequently administered. We intravenously delivered AAV1-X1 or X1.1 capsid packaging Ly6a into adult CBA/J mice. After 3 weeks of expression, we then injected PHP.eB packaging eGFP into the same mice (Fig. 4A, D). We observed increased eGFP expression in the brains of CBA/J mice injected with AAV1-X1: CAG-Ly6a but not the mice injected with X1.1: CAG-Ly6a, indicating that AAV1-X1 enables the subsequent administration of PHP.eB and also facilitates the permeability of PHP.eB (Fig. 4D). This result indicates that the serotype switching paradigm enabled by AAV1-X1 could potentially provide a solution for AAV re-administration in mice.

Fig. 2 | Semi-rational refinement of X1's tropism by further cargo and capsid engineering. A Illustration demonstrating cargo and capsid engineering to refine X1's tropism to increase brain targeting and lower liver targeting. Created with BioRender.com. **B** Representative images of vector-mediated expression of eGFP (green) in hippocampus and liver. Images are matched in fluorescence intensity to the X1: CAG-eGFP image. Brain scale bar: 100 μm. Liver scale bar: 2 mm. (n = 4 per group, 8-week-old C57BL/6J males, 3×10^{11} vg IV dose per mouse, 3 weeks of expression). (Top left) X1-mediated expression of CAG-eGFP. (Bottom left) X1-mediated eGFP expression with cargo engineering by incorporating MicroRNA-122 target sites (miR122TSS) in the CAG-eGFP genome. (Top right) Further capsid engineering by substitution at AA 452–458 of AAV-X1 yielding X1.1, X1.2, and X1.3. (Bottom right) Further capsid engineering on AAV-X1 by mutating AA272/AA386/AA503 to alanine to yield X1.4, X1.6, and X1.5, respectively. **C** (Left) Percentage of AAV-mediated eGFP-expressing cells that overlap with GLUT1+ markers across brain regions, representing the efficiency of the vectors' targeting of GLUT1+ cells.

A two-way ANOVA and Tukey's multiple comparisons tests with adjusted *P* values are reported (***P = 0.0002 for X1 versus X1.1 in the cortex, **P = 0.0022 for X1 versus X1.1 in the hippocampus, **P = 0.0049 for X1 versus X1.1 in the thalamus). Each data point shows the mean of three slices per mouse. (Right) Percentage of GLUT1+ markers in AAV-mediated eGFP-expressing cells across brain regions, representing the specificity of the vectors' targeting of GLUT1+ cells. A two-way ANOVA and Tukey's multiple comparisons tests with adjusted *P* values are reported (**P = 0.0013 for X1 versus X1.1 in the cortex, n.s. *P* = 0.3854 for X1 versus X1.1 in the hippocampus, *P = 0.0413 for X1 versus X1.1 in the thalamus). Each data point shows the mean of three slices per mouse. **D** AAV vector yields. A two-way ANOVA and Tukey's multiple comparisons tests with adjusted *P* values are reported (**P = 0.0012 for AAV9 versus AAV-X1, n.s. *P* > 0.9999 for AAV9 versus AAV-X1.1; n = 5 per group, each data point is the mean of three technical replicates, mean ± SEM is plotted). Source data are provided as a Source Data file.

The X1.1 vector can transform brain endothelial cells into a biofactory for secreted protein delivery to the brain

The broad distribution of vasculature across brain regions creates the opportunity to transform endothelial cells into a biofactory for the broad production of therapeutic agents, such as secreted proteins with trophic properties for other cell types within the CNS. For secreted proteins, this would remove the production burden from the target cell, which may already reside in a disease state. Since our novel vectors transduce brain endothelial cells efficiently and specifically, they provide a unique tool for us to explore this concept.

Sparc-like protein 1 (Sparcl1), which is also known as Hevin, is a matricellular secreted protein that is predominantly expressed by astrocytes and a subset of neurons in the CNS. Endothelial cells also express Sparcl1 mRNA; however, protein expression by these cells has not been observed[48,49]. Downregulation or missense mutations in SPARCL1/Hevin have been reported in numerous neurological disorders such as autism, schizophrenia, and depression[50–52]. In the developing mouse visual cortex, Hevin is specifically required for the formation and plasticity of thalamocortical connections[27,28]. Hevin knockout mice (Hevin KO) display a dramatic loss of Vesicular Glutamate Transporter 2 positive (VGluT2+) thalamocortical synapses both in the first three postnatal weeks and as adults (Fig. 4E)[27].

To determine if ectopic expression of Hevin by CNS endothelial cells can rescue the deficits observed in Hevin-KO mice, we generated a viral vector for Hevin expression using our capsid AAV-X1.1. Indeed, AAV-X1.1 packaging Hevin efficiently transduced brain endothelial cells and drove the expression of Hevin in these cells. To investigate whether Hevin production via endothelial cells would rescue the deficits in thalamocortical synapses observed in Hevin-KO mice, we retro-orbitally delivered both Hevin-HA and eGFP driven by the CAG promoter into 4-month-old Hevin-KO mice (Fig. 4E). After 3 weeks, we observed robust and specific expression of transgenes in brain endothelial cells (Fig. 4F and Supplementary Fig. 4B, C). Further, a synapse assay using the presynaptic thalamocortical marker VGluT2 and postsynaptic marker PSD95 in Hevin-KO mice showed a significantly higher number of thalamocortical synapses in layer IV of the V1 cortex in the treated group (CAG-Hevin) compared to the control (CAG-eGFP) (Fig. 4G). This result indicates that the Hevin produced and secreted from the brain endothelial cells was able to mimic endogenous Hevin function, rescuing the thalamocortical synapse formation that is severely deficient in Hevin-KO mice. This system thus illustrates a potential therapeutic strategy for Hevin-related disorders.

The X1 vector family efficiently transduces human brain endothelial cells in vitro

After validating the novel vectors' transduction profiles and demonstrating their functional application in rodent species, we next explored translation to higher organisms. We measured the performance of X1 in transducing isolated human brain microvascular

endothelial cells (HBMECs). At an MOI of 3×10^4, X1 transduced ~42% of HBMECs, ~180-fold higher than its parent AAV9. The further-engineered versions X1.1 and X1.2 transduced 44 and 53% of HBMECs, respectively. In contrast, previously-engineered AAV vectors, including PHP.eB and BR1 transduced ~0–2% of HBMECs, showing no obvious improvement in transduction compared to natural serotypes (Fig. 5A). AAV1-X1 and AAV-DJ-X1 also showed improvement in transduction of HBMECs compared to their parent serotype, respectively (Supplementary Fig. 4D). We next examined the vectors' performance at a lower MOI of 3×10^3 and again observed an improvement in transduction efficiency for X1.1 and X1.2, which transduced ~22% and ~28% of HBMECs (Fig. 5A). In addition to transducing HBMECs, X1, and its engineered derivatives exhibited robust transduction of multiple other human-derived cell lines, including HeLa, U87, and IMR32 (Supplementary Fig. 4E).

X1.1 efficiently transduces cultured ex vivo brain slices from macaque and human

The strong performance of the novel vectors in HBMECs prompted us to investigate their efficacy in a system that may better mimic in vivo conditions in non-human primates. We thus turned to an ex vivo brain slice culture system (Fig. 5B)[53]. The slices were freshly extracted from primate brains and cultured ex vivo. The versatile nature of this ex vivo system provides us with a rare opportunity to compare most of the CNS-tropic AAVs engineered in our lab in the same conditions in primate tissue. We packaged CAG-Frataxin(FXN)-HA with unique 12 bp barcodes in a panel of AAVs, including AAV9, X1.1, and several other engineered CNS-tropic AAVs. We then applied them both individually and together as a pool to brain slices freshly extracted from the southern pig-tailed macaque (*Macaca nemestrina*) and cultured in physiological conditions (Fig. 5B). After 7–10 days, we extracted DNA and RNA from the tissue, and calculated the enrichments of the variants from the AAV pool in the tissue using next-generation sequencing (NGS). X1.1 showed an ~4-fold increase and ~25-fold increase in DNA and RNA, respectively, compared to AAV9. This outperformed all other vectors, including CAP-B10 and CAP-B22, which have been shown to have increased efficiency in transducing the CNS of marmosets after systemic delivery[14] (Fig. 5C). The previously-reported MaCPNS2, which has increased targeting of the macaque CNS, also showed an ~5-fold increase in RNA compared to AAV9[10] (Fig. 5C). We also observed a higher DNA and RNA presence of X1.1 compared to other AAVs in the pool in the rhesus macaque brain (Supplementary Fig. 5A, B). Immunohistochemistry (IHC) staining of the HA tag confirmed the robust transduction by X1.1 in pig-tailed macaque (Fig. 5D and Supplementary Fig. 5C). Interestingly, X1.1-induced protein expression in the ex vivo brain slices were mostly seen in neurons (Fig. 5D and Supplementary Fig. 5D). RNAscope experiments revealed that some X1.1-delivered GFP mRNA transcripts were also observed in GLUT1+ cells while most of them remained in neurons (Supplementary Fig. 5E, F).
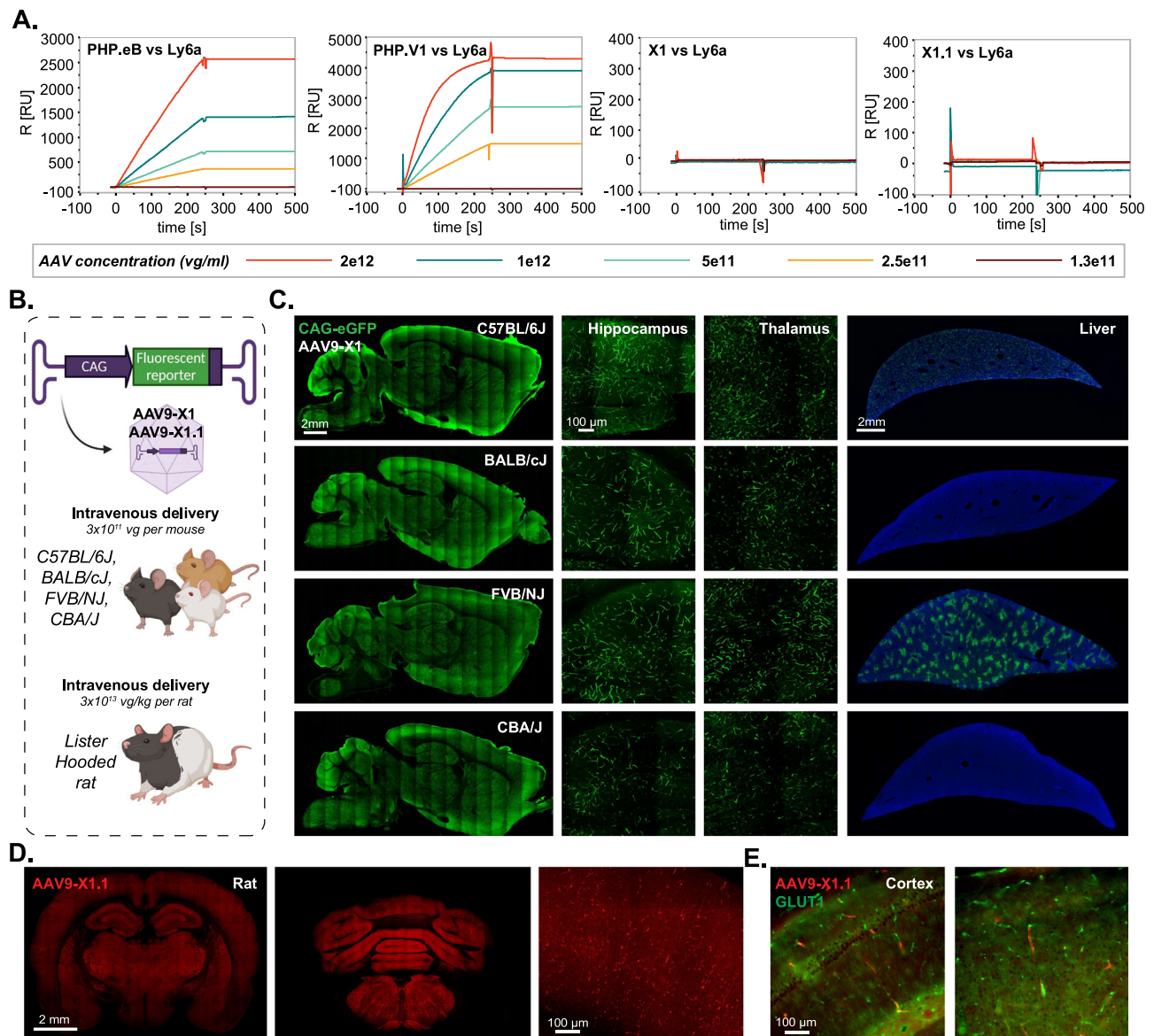
Fig. 3 | AAV9-X1 and AAV9-X1.1 efficiently transduce brain endothelial cells across diverse mice strains and rats. A Surface plasmon resonance (SPR) plots of PHP.eB, PHP.V1, AAV-X1, and AAV-X1.1 binding to surface-immobilized Ly6a-Fc protein captured on a protein A chip. Lines show the binding response for each vector across a range of vector concentrations. **B** Illustration demonstrating the IV administration of AAV-X1 capsid packaged with ssAAV:CAG-eGFP genome in genetically diverse mice strains (~8-week-old young C57BL/6J, BALB/cJ, FVB/NJ, and CBA/J, 3E11 vg per mouse) and IV administration of AAV-X1.1 capsid packaged with ssAAV:CAG-tdTomato genome in Lister Hooded rats (adult, 3E13 vg per rat). Created with BioRender.com. **C** Representative brain and liver images of AAV-X1-mediated eGFP expression (green) in C57BL/6J, BALB/cJ, FVB/NJ, and CBA/J mice with zoomed-in images of hippocampus and thalamus. $N = 4$ for each mouse strain, males and females, 3 weeks of expression. Sagittal brain section scale bar: 2 mm. Hippocampus and thalamus scale bar: 100 μm. Liver scale bar: 2 mm. **D** Representative images of the forebrain and hindbrain of AAV-X1.1-mediated tdTomato expression (red) in female Lister Hooded rat. Scale bar: 2 mm, zoom-in image scale bar: 100 μm. $N = 3$ rats were tested, 3 weeks of expression. **E** Representative images of cortex of AAV-X1.1-mediated tdTomato expression (red) in female Lister Hooded rat. Tissues were co-stained with GLUT1 (green). $N = 3$ rats were tested, 3 weeks of expression.

We then performed similar testing on human brain slices originating from a biopsy surgery. X1.1 showed an ~5-fold and ~33-fold increase in DNA and RNA, respectively, compared to AAV9, again outperforming several previously-engineered CNS-targeting vectors (Fig. 5E). The strong performance of X1.1 across macaque and human ex vivo slices (Fig. 5F) suggests great potential for the capsid in future translational applications.

X1.1 efficiently targets the CNS in rhesus macaque following IV delivery

Having validated the new variants' transduction profiles in ex vivo NHP and human brain models, we decided to investigate their efficacy

in vivo. We first tested them in the marmoset, a New World monkey. To reduce animal subject numbers, we simultaneously tested two viral capsids (AAV9 and X1.1) packaging different fluorescent reporters (either ssAAV:CAG-eGFP or ssAAV:CAG-tdTomato) in each adult marmoset (Supplementary Fig. 6A). Three weeks after IV delivery of the viruses, we observed no obvious differences between the CNS transduction of X1.1 and AAV9 (Supplementary Fig. 6B, C). This result emphasizes again that BBB heterogeneity should be taken into account when performing AAV engineering.

We then tested their efficacy in the rhesus macaque, an Old World monkey. We intravenously injected a pool of AAV9 and X1.1, each packaging a unique barcode, into a neonate rhesus macaque (male

Macaca mulatta, within 10 days of birth, 1×10^{13} vg/kg per AAV, $n = 1$ per group) (Supplementary Fig. 7A). After 4 weeks of expression, X1.1 showed an increase in vector genomes and RNA transcripts across brain regions include cortex, hippocampus, and cerebellum, compared to AAV9 (Supplementary Fig. 7B–D). In peripheral tissue such as the liver, muscle, and enteric system, X1.1 showed a reduction in both DNA and RNA compared to AAV9 (Supplementary Fig. 7B–D). After

seeing X1.1's superior performance in targeting CNS while detargeting peripheral organs at DNA and RNA levels, we next examined its cell-type targeting profile in the CNS. We packaged ssAAV:CAG-eGFP in AAV9 and ssAAV:CAG-tdTomato in X1.1, then intravenously delivered them as an AAV cocktail to a neonate rhesus macaque (female *Macaca mulatta*, within 10 days of birth, 5×10^{13} vg/kg per macaque, 2.5×10^{13} vg/kg per AAV, $n = 1$ per group) (Fig. 6A). After 4 weeks of

Fig. 4 | X1 capsids can enable repeated AAV administration with serotype switching and can transform the BBB into a biofactory. A Illustration of utilizing serotype switching to increase BBB permeability for AAVs in non-permissive strains. Created with BioRender.com. **B** (Left) Illustration of AAV1 monomer structure with the position of the 7-mer insertion, AA 588/589, highlighted (red). (Right) Sequences of AAVs around the insertion site are shown. The color is based on physicochemical properties (Zappo). **C** (Top) Representative images of AAV1, AAV1-PHP.B, and AAV1-X1-mediated eGFP expression in the hippocampus (scale bar: 100 μm). (Bottom) Zoomed-in images of tissues co-stained with GLUT1 (white) and DAPI (blue) (scale bars: 50 μm). *N* = 3 mice were tested for each AAV, 3 weeks of expression. **D** (Left) Representative image of PHP.eB-mediated eGFP expression in the brain of CBA/J mice (scale bar: 200 μm). (Right) Representative images of the brains of CBA/J mice following sequential administration of either AAV9-X1.1:CAG-Ly6a or AAV1-X1:CAG-Ly6a followed by PHP.eB:CAG-eGFP. *N* = 4 mice were tested for each condition, 8 weeks old, male, 3e11 vg/mouse. **E** Illustration of transforming brain endothelial cells into a biofactory. (Bottom right) Illustration of the

thalamocortical synapses identified by co-localization of VGLUT2 and PSD95 staining. Thalamocortical synapses are lost in Hevin-KO mice. Created with BioRender.com. **F** (Top) Representative images of AAV-X1.1 vector-mediated expression of eGFP (green) in the brain, which were co-stained with GLUT1 (red) and DAPI (blue) markers (scale bars: 30 μm). (Bottom) Representative images of AAV-X1.1 vector-mediated expression of Hevin in the brain. The tissues were co-stained with HA (green), GLUT1 (red), and DAPI (blue) markers (scale bar: 30 μm). *N* = 4 males each group, 3 weeks of expression, 4-month-old Hevin-KO mice, 1e12 vg/mouse. **G** (Left) Representative images of cortical slices stained for PSD95 (green) and VGLUT2 (red) (scale bar: 5 μm). (Right) Quantification of colocalized puncta of VGLUT2 and PSD95 in mice. One-way ANOVA Brown-Forsythe test (****P = 9e-5 for WT versus Hevin-KO: CAG-eGFP, ***P = 0.0006 for Hevin-KO: CAG-eGFP versus Hevin-KO: CAG-Hevin, n.s. P = 0.1156 for WT versus Hevin-KO: CAG-Hevin; n = 4 per group, each data point is the mean of 15 slices for one animal, mean ± SEM is plotted). Source data are provided as a Source Data file.

expression, we observed robust expression of X1.1 across brain regions including cortex, lingual gyrus (LG), hippocampus, and cerebellum, compared to AAV9 (Fig. 6B, C and Supplementary Movie. 1). Further IHC staining revealed that ~98% of the cells transduced by X1.1 in the cortex were neurons, while a small proportion of the targeted cells were endothelial or glia cells (Fig. 6D, E). Neuron transduction by X1.1 was ~45-fold higher than AAV9 (Fig. 6F). The difference between the neurotropic profile of X1.1 in neonate macaque and its endothelial cell-tropic profile in rodents both opens up potential applications and highlights the necessity of profiling AAV vectors across species. These experiments demonstrate that the new capsid AAV-X1.1 can efficiently transduce the CNS in infant Old World monkeys, making it a potentially useful vector for research of neurological disorders.

Discussion

In this study, we describe a family of novel vectors, including AAV-X1 and AAV-X1.1, which specifically and efficiently transduces mouse brain endothelial cells with a ubiquitous promoter following systemic administration. The previously-engineered AAV vector PHP.eB[12] has been widely used for targeting most cell types in mouse CNS, while the more recently-engineered vector PHP.V1[13] has been shown to have increased potency for, but not selective targeting of, brain endothelial cells. However, the enhanced CNS tropism of both vectors is absent in a subset of mouse strains, including BALB/cJ. Here we show that, similar to PHP.eB, PHP.V1 relies on Ly6a, while AAV-X1 vectors are Ly6a-independent and efficiently target brain endothelial cells across mouse strains. This Ly6a independence suggests that these novel vectors may utilize a novel receptor for CNS targeting and adds to the vectors' translational promise, as Ly6a is a murine-specific factor.
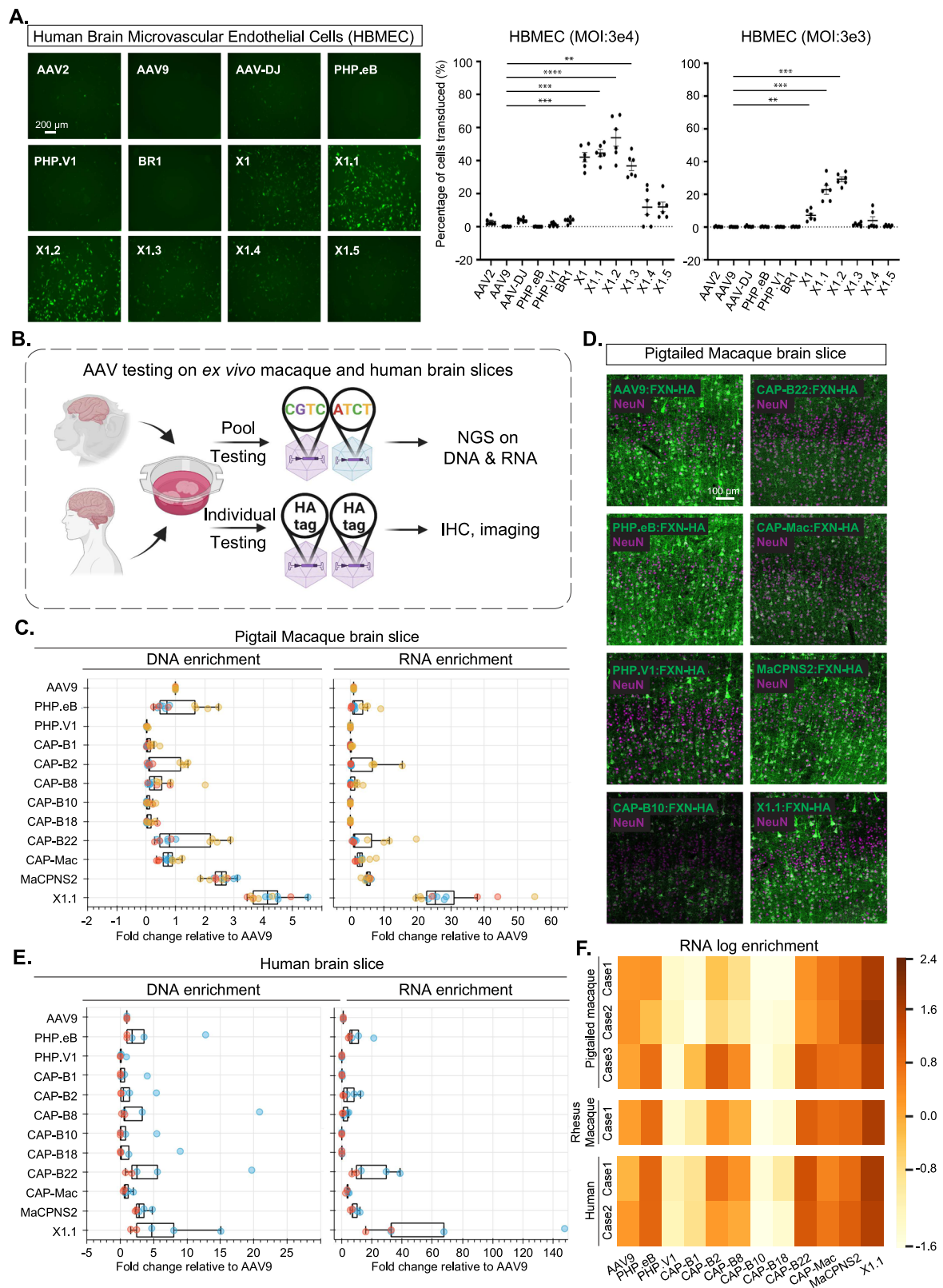
A major challenge in achieving successful gene therapy is the presence of neutralizing antibodies against AAVs. The neutralizing antibodies induced by an initial AAV delivery have been reported to persist long after the treatment, which could prevent the successful repeated administration needed for maintaining transgene expression[18]. Serotype switching between administrations could be a potential solution for dealing with neutralizing antibodies against the initially-administered serotype. We successfully transferred the 7-mer X1 peptide from AAV9 to AAV1, yielding AAV1-X1, which transduces brain endothelial cells efficiently following IV delivery. This result shows that the X1 peptide is more versatile than the 7-mer peptide of PHP.B[46]. Administering AAV1-X1 packaging Ly6a, we successfully made CBA/J mice more permissive for PHP.eB, thus both demonstrating the novel vector's ability to introduce a functional receptor and verifying that serotype switching may be a potential solution for sequential AAV administration[54,55]. The transferability of the AAV9-based X1's 7-mer peptide to AAV1 and AAV-DJ highlights a general strategy that could be applied to other engineered AAVs, although the previous failure of the transfer of PHP.B's CNS-tropic phenotype along with its peptide to AAV1[44–47] cautions that the success

of this strategy could vary case by case (Supplementary Table 1). Engineered AAVs in diverse serotype backbones could not only help with applications involving repeated administration but also circumvent pre-existing neutralizing antibodies to a certain AAV serotype.

Delivering therapeutic agents, or genetic material encoding therapeutics, across the BBB to treat neurological diseases of the CNS remains a challenging task[56,57]. Many enzymes, however, are secreted and can exert cross-correction effects. For these, we could instead deliver the genetic material to brain endothelial cells, transforming these cells into a biofactory to produce and distribute therapeutics to other cell types. The novel endothelial cell-tropic vector we describe here provided us with a unique chance to explore this concept in an animal model. We used the X1.1 vector to induce Sparcl1/Hevin protein production in brain endothelial cells and observed that this rescued the thalamocortical synapse loss phenotype of Hevin-KO mice. This proof-of-concept supports the brain endothelial cell biofactory model for the production of enzymes, antibodies, or other biological therapeutics, suggesting a novel therapeutic approach for diseases like lysosomal storage disorders.

Previous systemic AAVs for the CNS that were engineered in mice have not always translated to NHPs[38,58]. Tropism of previously-reported endothelial variants such as BR1[15] or BI30[59] remain unexplored in non-human primates. Given the X1 vectors' independence of Ly6a, we tested the novel vectors in various NHP species. We initially tested X1.1 in marmoset, a New World monkey, but did not observe an obvious difference in targeting the CNS compared to AAV9 following systemic delivery. We then turned to the macaque, an Old World monkey, which is more similar genetically to humans and is widely used in research, including gene therapy[9,60,61]. We first tested the virus on ex vivo brain slices from the rhesus macaque (*Macaca mulatta*) and southern pig-tailed macaque (*Macaca nemestrina*). We observed greater increases in DNA, RNA, and protein with X1.1 than other CNS vectors, including PHP.eB[12], CAP-B10, and CAP-B22[14]. We then intravenously injected X1.1 in the rhesus macaque and observed a significant improvement in targeting the CNS compared to AAV9. Interestingly, the rodent-endothelial-tropic X1.1 efficiently transduces neurons in the macaque brain. The conservation of enhanced CNS tropism across rodents and NHPs is encouraging for X1.1's potential in tackling neurological disorders in specific conditions. We further showed that our engineered vector X1.1 also has increased efficiency in transducing ex vivo adult macaque and human brain slices compared to other previously-engineered CNS vectors. Further experiments will be needed to examine the novel vectors' translation potential in adult primates.

The exact mechanism behind the distinction in the cell-type tropism of X1.1 across models tested remains unknown. The different ages of animals tested, the difference in BBB maturation, and the different routes of administration would also need to be taken into consideration for this distinction (Supplementary Table 2). In rodents

A. Human Brain Microvascular Endothelial Cells (HBMEC)

B. AAV testing on *ex vivo* macaque and human brain slices

C. Pigtail Macaque brain slice

D. Pigtailed Macaque brain slice

E. Human brain slice

F. RNA log enrichment

with a healthy BBB, X1 vectors seem to prefer endocytosis to transcytosis at the BBB, either due to their interactions with novel receptors or the vector's own physiological features. In pericyte-deficient mice where endothelial transcytosis is increased and endothelial cells show occasional hot-spot leakage areas due to altered endothelial cell-cell interaction[41,42], we observed increased transduction of astrocytes and neurons. In rhesus macaque, X1.1 seems biased towards transcytosis at

the BBB and transduces neurons efficiently after crossing the BBB. This distinction in tropism opens up the potential for different applications with X1.1 in endothelial cells and neurons in different species. It also emphasizes the need to test AAV variants across species to capture their complete profile.

In summary, here we describe systemic AAV tools for expanding our understanding of the neurovascular unit across species. The novel

Fig. 5 | Engineered AAVs can efficiently transduce cultured human brain microvascular endothelial cells and ex vivo macaque and human brain slices.
A (Left) Representative images of AAV (AAV2, AAV9, AAV-DJ, PHP.eB, PHP.V1, BR1, X1, X1.1, X1.2, X1.3, X1.4, X1.5)-mediated eGFP expression (green) in human brain microvascular endothelial cells (HBMECs). (AAVs packaged with ssAAV:CAG-eGFP, n = 6 per condition, 1-day expression). (Right) Percentage of cells transduced by the AAVs. In the condition of MOI:3E4, one-way ANOVA nonparametric Kruskal–Wallis test and multiple comparisons with uncorrected Dunn's test are reported (***P = 0.0004 for AAV9 versus AAV-X1, ***P = 0.0002 for AAV9 versus AAV-X1.1, ****P = 3.3e-5 for AAV9 versus AAV-X1.2, **P = 0.002 for AAV9 versus AAV-X1.3). In the condition of MOI:3E3, one-way ANOVA nonparametric Kruskal–Wallis test and multiple comparisons with uncorrected Dunn's test are reported (**P = 0.0082 for AAV9 versus AAV-X1, ***P = 0.0004 for AAV9 versus AAV-X1.1, ***P = 0.0001 for AAV9 versus AAV-X1.2). n = 6 per group, each data point is the mean of three technical replicates, mean ± SEM is plotted. **B** Illustration of AAV testing in ex vivo

macaque and human brain slices. Created with BioRender.com. **C** DNA and RNA levels in southern pig-tailed macaque brain slices for AAVs, with DNA and RNA levels normalized to AAV9. N = 12 independent slices were examined over three pig-tailed macaque cases. Box plots represent the median, the first quartiles and third quartiles, with whiskers drawn at the 1.5 IQR value. Points outside the whiskers are outliers. **D** Representative images of AAV-mediated CAG-FXN-HA expression in ex vivo southern pig-tailed macaque brain slices. N = 12 independent slices were examined over three pig-tailed macaque cases. The tissues were co-stained with antibodies against HA (green) and NeuN (magenta). **E** DNA and RNA level in human brain slices for AAVs, with DNA and RNA levels normalized to AAV9. N = 5 independent slices were examined over two human cases. Box plots represent the median, the first quartiles and third quartiles, with whiskers drawn at the 1.5 IQR value. Points outside the whiskers are outliers. **F** RNA log enrichment of AAVs across three pig-tailed macaques, one rhesus macaque, and two human brain cases. Source data are provided as a Source Data file.

vector X1 and its further-engineered family of variants, including X1.1, provide genetic access to brain endothelial cells in mice with high potency and specificity, and their efficient targeting of the CNS in NHP and human brain slices offers hope of accelerating translational research. The surprising transferability of the X1 AAV9 variant peptide to other AAV serotypes can allow researchers to apply immunogenically-distinct AAVs at multiple timepoints, and the demonstrated application of the X1 vectors to transform mouse brain endothelial cells into a secretory biofactory validates a novel method to test preclinical agents for CNS therapies.

Methods
Plasmids
Library preparation. The plasmids used for AAV library preparation were described previously. Plasmid rAAV-ΔCap-in-cis-Lox2 was used for building the heptamer insertion (7-mer-i) AAV library. Plasmid pCRII-9Cap-XE was used as a PCR template for the DNA library generation. Plasmid AAV2/9-REP-AAP-ΔCap was used to supplement the AAV library during virus production[7,10,13].

DNA constructs for AAV characterization. The AAV capsid AAV-X1 was built by inserting 7-mer peptides between AAs 588-589 of the AAV9 cap gene in the pUCmini-iCAP-PHP.B backbone[13]. The AAV-PHP.V1 capsid was described previously (Addgene 127847)[13]. The AAV capsid AAV-X1.1 (Addgene 196836), AAV-X1.2, and AAV-X1.3 were built by substituting AAs 452–458 of AAV-X1. The AAV capsids AAV-X1.4, AAV-X1.5, and AAV-X1.6 were built by mutation of AA272/386/503 in AAV-X1 to Alanine. The AAV capsid AAV1-X1 was built by inserting a 7-mer peptide between AAs 588-589 of the AAV1 cap gene in AAV1-Rep-Cap (Addgene 112862)[62]. Please refer to Supplementary Table 1 for more details.

For in vivo validation of AAV capsids, we packaged the vectors with a single-stranded (ss) rAAV genome: pAAV:CAG-eGFP, pAAV:CAG-tdTomato (a gift from Edward Boyden, Addgene plasmid # 59462). To make pAAV:CAG-eGFP-3xMir122-TS, three copies of the Mir122-TS were cut out from plasmid CAG-GCaMP6f-3x-miR204-5p-3x-miR122-TS[62]. To make pAAV:CAG-Hevin-HA, Hevin-HA was synthesized as a gBlocks Gene Fragment (IDT) based off the sequence in the plasmid pAAV:GfaABC1D-Hevin, a gift from Cagla Eroglu's Lab, and subcloned into the plasmid pAAV:CAG-eGFP by replacing the eGFP gene. To make pAAV:CAG-Ly6a, the Ly6a coding sequence from C57BL/6J was synthesized as a gBlocks Gene Fragment (IDT) and subcloned into the plasmid pAAV:CAG-eGFP by replacing the eGFP gene. pAAV-CAG-FXN-HA was chosen for the ex vivo slice study because it contains a ubiquitous CAG promoter and an HA-tagged endogenous human frataxin (FXN) protein-coding sequence and a unique 12 bp barcode sequence. The barcode sequence was used to differentiate different capsids packaging the same construct during the next-generation sequencing (NGS) analysis.

AAV capsid library generation. The round-1 (R1) and round-2 (R2) libraries were generated as described previously in refs. 10, 13. Briefly, the R1 library involved a randomized 21-nucleotide (7xNNK mutagenesis) insertion between AAs 588-589 of the AAV9 capsid. The R2 library was built using a *synthetic pool* method[10,13].
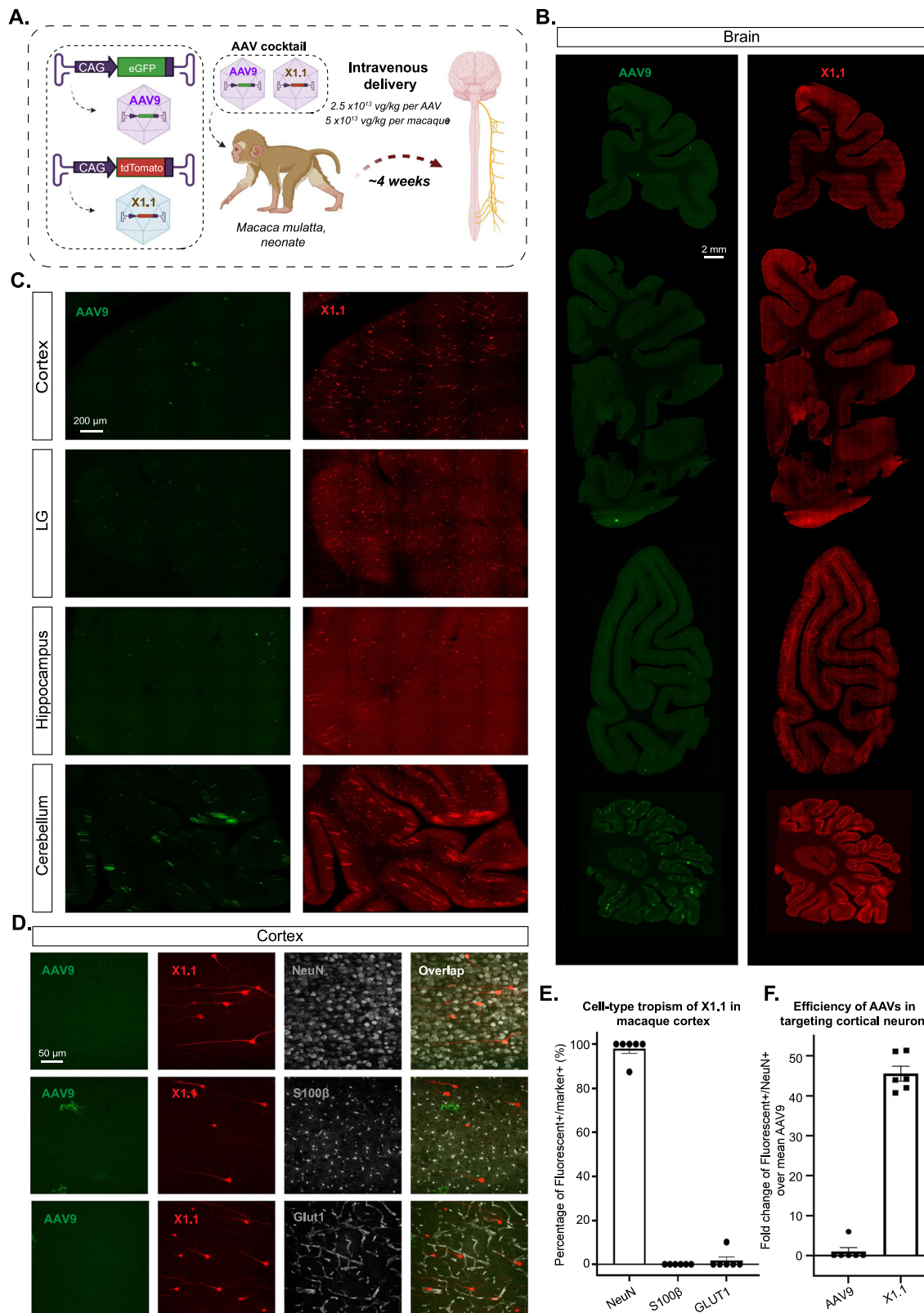
Animals and subjects
All animal procedures in mice that were carried out in this study were approved by the California Institute of Technology Institutional Animal Care and Use Committee (IACUC), Caltech Office of Laboratory Animal Resources (OLAR), Cantonal Veterinary Office Zurich (license number ZH194/2020, 32869/2020), and Duke Division of Laboratory Animal Resources (DLAR). All experimental procedures in rats were conducted at UCL according to the UK Animals Scientific Procedures Act (1986) and under personal and project licenses granted by the Home Office following appropriate ethics review. For mouse studies, we purchased C57BL/6J (000664), BALB/cJ (000651), FVB/NJ (001800), CBA/J (000656), and Tek-Cre (008863) mice (both male and females, 6–8 weeks or 2 years old) from the Jackson Laboratory. 4-month-old male Hevin-KO mice[26] were injected at Duke University. 4–5-month-old female Pdgfb ret/ret mice[63] were injected at the University of Zurich. Mice were housed under standard conditions between 71 and 75 °F, in 30–70% humidity, and on a light cycle of 13 h on and 11 h off.

All experimental procedures performed on marmosets were approved by the University of California, San Diego, Institutional Animal Care and Use Committee (IACUC) and in accordance with the National Institutes of Health and the American Veterinary Medical Association guidelines. 16-month-old marmosets (one female animal and one male animal) were used in this study and received intravenous injections of AAVs.

All experimental procedures performed on rhesus macaques were approved by the International Animal Care and Use Committee at the University of California, Davis and the California National Primate Research Center (CNPRC). One infant female animal and one infant male animal were used in this study. Both received intravenous injections of AAVs within 10 days of birth.

All human neurosurgical tissue studies were approved by the Western Institutional Review Board. Human neurosurgical specimens were obtained with the informed consent of patients that underwent neocortex resection for tumor removal. In order to gain access to deep brain tumors, surgeons need to remove some peri-tumor tissue from the cortex of the patients. These specimens, which were distal to the pathological focus of the surgical resections, were not required for diagnosis and were reallocated for research[64].

For all the experiments performed in this study, the animals were randomly assigned, and the experimenters were not blinded while performing the experiments unless mentioned otherwise.

In vivo selection and capsid library recovery

For capsid selection in vivo, the virus library was intravenously administered to male and female mice of various Cre transgenic lines ($n = 3$ per Cre line) at 3×10^{11} vg per mouse in R1 selection, and at 3×10^{11} vg per mouse in R2 selection. rAAV genomes were recovered by Cre-dependent PCR or Cre-independent PCR as previously described in ref. 13. The AAV DNA library, virus library, and the libraries recovered from tissue post-in vivo selection were processed for NGS as also described previously in refs. 10,13.

Characterization of AAV vectors across models

AAV vector production. The AAV vectors were produced using an optimized vector production protocol[62]. Plasmids were transfected into HEK 293 T cells (ATCC) using polyethylenimine. We collected the

Fig. 6 | Engineered AAVs can efficiently transduce the central nervous system in the rhesus macaque. A Illustration of AAV vector delivery to rhesus macaque to study transduction across the CNS and PNS after 3 weeks of expression. Created with BioRender.com. The capsids (AAV9/X1.1) and their corresponding genomes (ssAAV:CAG-eGFP/tdTomato) are shown on the left. Two AAVs packaged with different fluorescent proteins were mixed and intravenously injected at a dose of 5×10^{13} vg/kg per macaque (*Macaca mulatta*, injected within 10 days of birth, female, i.e., 2.5×10^{13} vg/kg per AAV). Representative images of macaque **B**, coronal sections of the forebrain, midbrain, hindbrain, and cerebellum (scale bar: 2 mm), and **C**, selected brain areas: cortex, lingual gyrus (LG), hippocampus, and cerebellum (scale bar: 200 μm). **D** Brain tissues were co-stained with NeuN (white) or S100β (white) or GLUT1 (white); representative images of the cortex are shown. **E** Cell type tropism of X1.1 in the macaque brain, shown by the percentage of Fluorescent+/Marker+. Each data point is an average of three images from a slice, *n* = 6 slices from one rhesus macaque were examined. Mean ± SEM is plotted. **F** Quantification of the fold change of Fluorescent+/NeuN+ over mean AAV9 in the macaque brain. Each data point is an average of three images from a slice, *n* = 6 slices from one rhesus macaque were examined. Mean ± SEM is plotted. Source data are provided as a Source Data file.

medium 72 h after the transfection and harvested both the cells and medium 120 h after transfection. We precipitated the viral particles from the medium with 40% polyethylene in 500 mM NaCl and combined them with cell pellets for processing. The cell pellets were later suspended with 100 U/mL of salt-activated nuclease in 500 mM NaCl, 40 mM Tris, and 2.5 mM MgCl$_2$. AAVs were then harvested from the cell lysates with iodixanol step gradients and ultracentrifugation. Afterward, AAVs were concentrated with Amicon filters and formulated in a sterile PBS solution. Transmission electron microscopy (TEM) was used to examine the purity of the prep. The virus titer was measured by qPCR. The average yield was ~1×10^{12} vg per plate. BR1:CAG-eGFP was purchased from Signagen (SL116035).

AAV vector administration in mice and tissue harvest. For the cell-type profiling of the novel AAVs in mice, the AAV vectors were injected intravenously via the retro-orbital route to 6–8-week-old adult mice at a dose of $0.1–1 \times 10^{12}$ vg per mouse. The retro-orbital injections were performed as described previously in refs. [62], [64]. The expression times were ~3 weeks from the time of injection. The dosage and expression time were kept consistent across different experimental groups unless noted otherwise. To harvest the tissues of interest, the mice were anesthetized with Euthasol (pentobarbital sodium and phenytoin sodium solution, Virbac AH) and transcardially perfused using 30–50 mL of 0.1 M phosphate-buffered saline (PBS) (pH 7.4), followed by 30–50 mL of 4% paraformaldehyde (PFA) in 0.1 M PBS. The organs were collected and post-fixed 24–48 h in 4% PFA at 4 °C. Following this, the tissues were washed with 0.1 M PBS twice and stored in fresh PBS-azide (0.1 M PBS containing 0.05% sodium azide) at 4 °C.

In the Hevin experiment, 4-month-old Hevin-KO mice[26] were retro-orbitally injected with either AAV-X1.1:CAG-Hevin-HA or AAV-X1.1:CAG-eGFP (1E12 vg per mouse). After 3 weeks, the mice were perfused and brains were extracted for synapse assay. In the experiment with pericyte-deficient mice, 4–5-month-old PDGFB-retention motif knock-out mice (*Pdgfb$^{ret/ret}$*) in a C57BL6/J genetic background[63] were used. 3E11 vg per mice for X1 and 1E12 vg per mice for X1.1 were injected into mice via the tail vein. Three weeks post-injection, the anesthetized animals were perfused for 1–2 min with PBS, followed by 5 min perfusion with 4% PFA in PBS, pH 7.2. Brains were collected and post-fixed in 4% PFA in PBS, pH 7.2 at 4 °C for 6 h.

AAV vector administration in rat and tissue harvest. Female rats were used (150–200 g) for the experiments. 1E13 vg of the virus was delivered intravenously through the tail vein under light anesthesia. The injected volume was 0.5 ml containing the required number of particles. After 21 days, the animals were perfused using 4% PFA solution and PBS. Brains were collected.

AAV vector administration in marmoset and tissue harvest. The procedure we took was similar to our prior work[10]. Marmoset monkeys were anesthetized using an intramuscular Ketamine (20 mg/kg) and Acepromazine (0.5 mg/kg) injection. An intravenous catheter was placed in the saphenous vein of the hind leg and flushed with ~2 mL of LRS (Lactated Ringer's solution) for 2 min. Viruses were pooled together in a single syringe (~500–900 μL) and infused at a rate of 200 μL/min

into the catheter. Following the infusion, the catheter was flushed with ~3 mL of LRS for 2 min and removed. The animal was then returned to a recovery cage. Following an incubation period of 4-6 weeks post viral injection, the animals were euthanized by injecting pentobarbital intraperitoneally. Tissue was fixed in 4% PFA solution for estimation of protein expression.

AAV vector administration in macaque and tissue harvest. The procedure we took was similar to our prior work[10]. One female rhesus macaque was injected within 10 days of birth. Prior to injection, the animal was anesthetized with ketamine (0.1 mL) and the skin over the saphenous vein was shaved and sanitized. AAVs (2.5×10^{13} vg/kg) were slowly infused into the saphenous vein for ~1 min in <0.75 mL of 0.1 M PBS. The animal was monitored while they recovered from anesthesia in their home enclosure, and daily for the remainder of the study. The monkey was individually housed within sight and sound of conspecifics[10].

Tissues were collected 4 weeks post-AAV administration. The animal was deeply anesthetized and euthanized using sodium pentobarbital in accordance with guidelines for humane euthanasia of animals at the CNPRC. The whole body was perfused with ice-cold RNase-free 0.1 M PBS. The brain was removed from the skull and blocked into 4 mm thick slabs in the coronal plane. Brain slabs and organs were subsequently post-fixed in 4% PFA for 48 h. One hemisphere of the animal was cryoprotected in 10, 15, and 30% sucrose in 0.1 M PBS[10].

AAV vector administration in ex vivo human and non-human primate brain slices. All procedures involving non-human primates conformed to the guidelines provided by the US National Institutes of Health. Ex vivo brain slice culture experiments were performed on temporal cortex tissue from adult *Macaca nemestrina* or *Macaca mulatta* animals housed at the Washington National Primate Research Center. We obtained these brain samples through the Tissue Distribution Program operating under approved University of Washington IACUC protocol number 4277-01. For *Macaca nemestrina*, one male (7 years 5 months) and two females (2 years 9 months and 15 years 2 months) were used. For *Macaca mulatta*, one female (7 years 10 months) was used.

All human neurosurgical tissue studies were approved by the Western Institutional Review Board. Recruitment of the patients is performed outside of the supervision of the Allen Institute by a hospital-appointed case coordinator under the authority of the IRB of the participating hospital. Brain tissue was collected based on availability, both female and male tissue was used in this study. Human brain tissue in this paper came from peri-tumor tissue removed from the right parietal cortex of a 55-year-old female patient and the right frontal cortex of a 61-year-old male patient to access deep brain tumors. Human neurosurgical specimens were obtained with the informed consent of patients that underwent neocortex resection for the treatment of temporal lobe epilepsy or for tumor removal. In order to gain access to deep brain tumors, surgeons need to remove some peri-tumor tissue from the cortex of the patients. These specimens, which were distal to the pathological focus of the surgical resections, were not required for diagnosis and were reallocated for research[65].

Human and macaque brain slices were prepared using the NMDG protective recovery method[53,66]. Human neurosurgical tissue or macaque brain tissue specimens were placed in carbogenated NMDG artificial cerebral spinal (ACSF) solution containing (in mM): 92 NMDG, 2.5 KCl, 1.25 NaH₂PO₄, 30 NaHCO₃, 20 HEPES, 25 glucose, 2 thiourea, 5 Na-ascorbate, 3 Na-pyruvate, 0.5 CaCl₂.4H₂O, and 10 MgSO₄.7H₂O. Brain slices were prepared on a VF-200 Compresstome at 300-µm thickness using a zirconium ceramic blade (EF-INZ10, Cadence) and then underwent warmed recovery in carbogenated NMDG aCSF at 32–34 °C for 12 min. Human and macaque brain slices were placed on membrane inserts in six-well sterile culture plates, and wells were filled with slice culture medium consisting of 8.4 g/L MEM Eagle medium, 20% heat-inactivated horse serum, 30 mM HEPES, 13 mM D-glucose, 15 mM NaHCO₃, 1 mM ascorbic acid, 2 mM MgSO₄.7H₂O, 1 mM CaCl₂.4H₂O, 0.5 mM GlutaMAX-I, and 1 mg/L insulin[53]. The slice culture medium was carefully adjusted to pH 7.2–7.3, osmolality of 300–310 mOsmoles/kg by the addition of pure H₂O, and then sterile-filtered. Culture plates were placed in a humidified 5% CO₂ incubator at 35 °C and the slice culture medium was replaced every 2–3 days until endpoint analysis. One to three hours after plating, brain slices were infected by direct application of ~2.5 × 10¹⁰ vg of concentrated AAV viral particles distributed over the slice surface.

AAV vector characterization in cell cultures. Human brain microvascular endothelial cells (HBMECs) (ScienCell Research Laboratories, cat. no. 1000) were cultured as per the instructions provided by the vendor. The viral vectors packaging ssAAV: CAG-eGFP were added to the cell culture at a multiplicity of infection (MOI) of either 5E4 or 5E3 per well (six wells per dose per vector). The culture was assessed for fluorescence expression at 1-day post-infection. In the in vitro Ly6a experiment, HEK293T cells (ATCC, CRL-3216) were cultured in a six-well plate, Ly6a was transiently expressed in HEK293T cells by transfecting each well with 2.53 µg plasmid DNA. Receptor-expressing cells were transferred to 96-well plates and transduced with AAV variants at an MOI of 3E4 or 3E3 per well. The culture was assessed for fluorescence expression at 1-day post-infection. HeLa cells (ATCC, CCL-2), U87 cells (ATCC, HTB-14), and IMR32 cells (ATCC, CCL-127) were cultured as per the instructions provided by the vendor. The viral vectors packaging ssAAV: CAG-eGFP were added to the cell culture at an MOI of 5E4 per well (three wells per dose per vector). The culture was assessed for fluorescence expression at 1-day post-infection.

Immunohistochemistry and imaging
In the AAV characterization experiment in mice, tissue sections, 100-µm thick, were first incubated in the blocking buffer (10% normal donkey serum (NDS), 0.1% Triton X-100, and 0.01% sodium azide in 0.1 M PBS, pH 7.4) with primary antibodies at appropriate dilutions (Anti-CD31 from Histonova Cat # DIA-310, diluted 1:100; Anti-podocalyxin from R&D Systems Cat # AF1556, diluted 1:100; Anti-CD13 from AbD Serotec, Cat # MCA2183EL, diluted 1:100; Anti-CNN-1 (Calponin 1) from Abcam, Cat # Ab46794, diluted 1:100; Anti-Collagen-IV, from AbD, Serotec Cat # 2150-1470, diluted 1:300; Anti-GFAP from Invitrogen, Cat # 13-0300, diluted 1:600; Anti-HA from Roche, Cat# 11867423001, diluted 1:200; Anti-GFP from Aves Labs, Cat# GFP-1020, diluted 1:500; Anti-GLUT1 from Millipore, Cat#07-1401, diluted: 1:500; Anti-S100β from Abcam, Cat# ab52642, diluted: 1:500; Anti-NeuN from Abcam, Cat# ab177487, diluted: 1:500) for 24 h at room temperature (RT) on a rocker. After primary antibody incubation, the tissues were washed one to three times with wash buffer 1 (0.1% Triton X-100 in 0.1 M PBS buffer, pH 7.4) over a period of 5–6 h in total. The tissues were then incubated in the blocking buffer with the corresponding secondary antibodies (Anti-mouse Alexa488 from Invitrogen, Cat# A-11001, diluted 1:1000; Anti-mouse Alexa555 from Invitrogen, Cat# A-21422, diluted 1:1000; Anti-rabbit Alexa555 from Invitrogen, Cat# A-21428, diluted 1:1000; Anti-rabbit Alexa647

from Invitrogen, Cat# A-21245, diluted 1:1000; Anti-rat Alexa488 from Invitrogen, Cat# A-11006, diluted 1:1000; Anti-rat Alexa555 from Invitrogen, Cat# A-21434, diluted 1:1000; Anti-rabbit AF594 from Jackson Immuno, Cat# 711-585-152, diluted 1:1000) at RT and then washed 3 times in 0.1 M PBS over a total duration of 5–6 h. When performing DNA staining, the tissues were incubated with 4′, 6-diamidino-2-phenylindole (DAPI) (Sigma-Aldrich, 10236276001, 1:1000) in 0.1 M PBS for 15 min followed by a single wash for 10 min in 0.1 M PBS. The DAPI and/or antibody-stained tissue sections were mounted with ProLong Diamond Antifade Mountant (Thermo Fisher Scientific, P36970) before imaging them under the microscope. The images were acquired with a Zeiss LSM 880 confocal microscope using the following objectives: Plan-Apochromat 10× 0.45 M27 (working distance 2.0 mm), and Plan-Apochromat 25× 0.8 Imm Corr DIC M27 multi-immersion. The liver images were acquired with a Keyence BZ-X700 microscope using a 10x objective. The images were then processed in the following image processing softwares: Zen Black 2.3 SP1 (for Zeiss confocal images) and BZ-X Analyzer 1.4.0.1 (for Keyence images).

In the rat experiment, whole brains were imaged using serial section two-photon microscopy[67,68]. Our microscope was controlled by ScanImage Basic (Vidrio Technologies, USA) using BakingTray, a custom software wrapper for setting up the imaging parameters[69]. About 50–60 µm slices were cut and seven to nine optical planes were imaged using a 16x objective. Images were assembled using StitchIt[70].

In the Hevin experiment, for synaptic puncta analysis of the mouse primary visual cortex (area V1), brains were cryosectioned at 25 µm using Leica CM3050S (Leica, Germany). Tissue sections were washed and permeabilized in TBS with 0.2% Triton X-100 three times at room temperature, followed by blocking in 5% Normal Goat Serum (NGS) for 1 h at room temperature. To label pre and postsynaptic proteins, VGluT2 (Synaptic Systems; Cat# 135 404; diluted 1:500) and PSD95 (Thermo Fisher; Cat# 51-6900, diluted 1:500) antibodies were used, respectively. Primary antibodies were diluted in 5% NGS containing TBST and incubated overnight at 4 °C. Secondary antibodies (Alexa Fluor conjugated; Invitrogen) were added in TBST with 5% NGS for 2 h at room temperature. Slides were mounted in Vectashield with DAPI (Vector Laboratories, CA). Images were acquired with an Olympus FV3000 inverted confocal microscope using a high magnification 60x objective plus 1.64x optical zoom. Z-stack images contained 15 optical sections spaced 0.33 µm apart. During the post-processing of captured images, each z-stack was converted into five maximum-intensity projection (MIP) images by combining three optical sections using ImageJ software. The number of colocalized excitatory thalamocortical (VGluT2/PSD95) synaptic puncta was obtained using the ImageJ plugin Puncta Analyzer[71].

In the pericyte-deficient mouse experiment, coronal vibratome sections (60 µm) of brains were cut using the Leica VT1000S. Free-floating brain sections were incubated in the blocking/permeabilization solution (1% bovine serum albumin, 0.5% Triton X-100 in PBS) overnight at 4 °C, followed by incubation in primary antibody solution for two nights at 4 °C, and subsequently in secondary antibody solution, overnight at 4 °C. Sections were incubated with DAPI (4′,6-Diamidino-2-phenylindole dihydrochloride) solution (D9542, Sigma-Aldrich, diluted 1:10,000) for 7 min at RT and subsequently mounted in ProLong Gold Antifade mounting medium (cat. #P36930). Life Technologies). Images were taken with a Leica SP8 inverse, 20 X objective PL APO CS (NA 0.7) (Leica Microsystems). Widefield images were generated using Slidescanner Zeiss Axio Scan.Z1 (Leica Microsystems). Image processing was done using Fuji and Zen2. All confocal images are represented as maximum-intensity projections.

In the marmoset and macaque experiments, coronal sections (100 µm) of brains were cut using the Leica VT1000S. Sections (50–100 µm) of the gut, DRG, and spinal cord were cut using a cryostat (Leica Biosystems). Tissues were stained with relevant antibody following a similar protocol as in the mouse characterization experiment.

The images were acquired with a Zeiss LSM 880 confocal microscope using the following objectives: Plan-Apochromat 10× 0.45 M27 (working distance 2.0 mm) and Plan-Apochromat 25× 0.8 Imm Corr DIC M27 multi-immersion. The images were then processed in the Zen Black 2.3 SP1 (for Zeiss confocal images). The video was processed in Imaris 9 software.

In the primate ex vivo slice culture experiments, 7–10 days post-virus infection, temporal cortex brain slices were fixed in 4% PFA for 24 h at 4 °C. After PFA fixation, the slices were transferred into 30% sucrose in water for >24 h and then sub-sectioned on a sliding microtome to 15–30 μm for immunostaining using the following antibodies: mouse anti-HA (Biolegend catalog #901513, diluted 1:1000) and rabbit anti-NeuN (Millipore catalog #ABN78, 1:2000). In a subset of IHC experiments we performed co-immunostaining with additional cell type marker antibodies including the following: rabbit anti-GLUT1 (Millipore catalog #07-1401, diluted 1:1000), rabbit anti-Olig2 (Abcam catalog #AB9610, diluted 1:1000), and mouse anti-S100β (Millipore catalog #S2532, diluted 1:1000). We also switched from mouse anti-HA to rat anti-HA (Roche catalog # 11867423001, diluted 1:1000) to circumvent antibody cross-reactivity issues observed with Olig2 and other cell type markers. Then the tissues were incubated with corresponding secondary antibody (Anti-mouse Alexa488 from Invitrogen, Cat# A-11001, diluted 1:1000; Anti-mouse Alexa555 from Invitrogen, Cat# A-21422, diluted 1:1000; Anti-rabbit Alexa555 from Invitrogen, Cat# A-21428, diluted 1:1000; Anti-rabbit Alexa647 from Invitrogen, Cat# A-21245, diluted 1:1000; Anti-rat Alexa488 from Invitrogen, Cat# A-11006, diluted 1:1000; Anti-rat Alexa555 from Invitrogen, Cat# A-21434, diluted 1:1000) for 12 h in RT. After being rinsed in PBS solution, slices were incubated in 1 μg/mL DAPI solution and mounted on 1 × 3-inch slides with Prolong Gold mounting medium. Regions of interest (ROI) in the neocortical gray matter spanning L3/4/5 were imaged on an Olympus FV3000 confocal microscope using 405, 561, and 640 nm laser lines. Z-stack images were acquired at 1-um step size through the slice thickness and collapsed to make maximum-intensity projection images. Every attempt was made to select comparable ROIs in the brain slices that best captured viral reporter expression patterns and to image at matched settings to directly compare across the capsid variants. In some cases, images needed to be pseudo-colored post-acquisition to best illustrate signal overlap in two-channel merged images (green and magenta with an overlap in white).

In the RNAScope FISH and antibody labeling on ex vivo slice culture experiments, 350-μm thick macaque cortical slices were obtained, cultured, and transduced as above. After 8 days in culture, slices were fixed in 4% PFA (Electron Microscopy Sciences) at 4 °C for 12 h and cryoprotected in 30% sucrose. Thick slices were subsectioned with 15 μm thickness on a freezing sliding microtome (Leica SM2000R) and stored in 1 x phosphate-buffered saline (PBS) + 0.1% sodium azide at 4 °C. RNAscope Multiplex Fluorescent v2 (Advanced Cell Diagnostics) was performed, and if not otherwise noted, buffers or solutions were obtained from the ACD v2 kit. Sections were washed in 1 x PBS, mounted onto slides, and dried at 60 °C. Samples were fixed in 4% paraformaldehyde (PFA) for 15 min at 4 °C, followed by a series of 5 min washes in solutions with increasing ethanol concentrations (50, 70, 100, 100%). Hydrogen peroxide was applied and the sections were incubated at RT for 10 min, and washed in 1x PBS twice for 1 min. Samples were incubated in Target Retrieval Reagent for 5–7 min at 100 °C. Slides were rinsed in deionized water and incubated in 100% ethanol for 3 min and air-dried. A hydrophobic barrier around the tissue was created with an ImmEdge Pen (Vector Laboratories, H-4000). Samples were treated with Protease III for 30 min at 40 °C and then washed twice in 1x PBS for 1 min at RT. We used a C1 probe designed by ACD against SYFP2 for the detection of the EGFP reporter mRNA. Sections were incubated in this probe for 3 h at 40 °C. Sections were then washed twice in 1x Wash Buffer for 2 min each at RT, then incubated in 5x Sodium Chloride Sodium Citrate (SSC) (Invitrogen)

overnight at RT. Sections were incubated in Amp1 reagent for 30 min at 40 °C then washed twice in 1x Wash Buffer for 2 min at RT. Sections were then incubated in Amp2 reagent for 30 min at 40 °C, then washed twice in 1x Wash Buffer for 2 min at RT. Sections were then incubated in Amp3 reagent for 15 min at 40 °C, then washed twice in 1X Wash Buffer for 2 min at RT. Sections were then incubated in HRP-C1 at 40 °C for 15 min, washed twice in 1x Wash Buffer for 2 min at RT, then incubated in TSA Cy3 (Perkin Elmer, diluted 1:1500 in TSA Buffer) for 30 min at 40 °C. Sections were then incubated in HRP Blocker at 40 °C for 30 min and washed twice in 1x Wash Buffer for 2 min each at RT. Sections were washed in 1x PBS for 2 min at RT, then fixed in 4% PFA for 15 min at RT. Sections were washed twice in 1x PBS for 5 min. Next, slides were incubated in a blocking buffer of 10% normal goat serum (Jackson ImmunoResearch) in PBS for 15 min at RT. Sections were incubated in primary antibody for 1 h at RT: rabbit Anti-GLUT1 (Millipore), chicken Anti-GFP (Aves). Samples were then washed twice in 1x PBS for 5 min each, then incubated in secondary antibody for 1 h at RT: goat anti-rabbit Alexa Fluor 488 (Thermo Fisher), goat anti-chicken Alexa Fluor 488 (Thermo Fisher). Samples were washed twice in 1x PBS for 5 min each, counterstained with DAPI for 30 s at RT, then mounted with Prolong Gold Antifade Mountant (Thermo Fisher Scientific, P36930). Samples were imaged on an Olympus confocal FluoView3000 using a 30x silicone immersion objective or a Nikon Ti2 epifluorescence microscope with a 20x objective. Montage images were stitched with the Olympus software (FV31S-SW), stacks were Z-projected and analyzed using FIJI. Images from the Nikon are not montages, but are from a single plane. All analysis was done in FIJI.

Protein production

Ly6a-Fc was produced in Expi293F suspension cells grown in Expi293 Expression Medium (Thermo Fisher Scientific) in a 37 °C, 5% CO_2 incubator with 130 rpm shaking. Transfection was performed with Expifectamine according to the manufacturer's instructions (Thermo Fisher Scientific). Following harvesting of cell-conditioned media, 1 M Tris, pH 8.0, was added to a final concentration of 20 mM. Ni-NTA Agarose (QIAGEN) was added to ~5% conditioned media volume. 1 M sterile PBS, pH 7.2 (GIBCO), was added to ~3X conditioned media volume. The mixture was stirred overnight at 4 °C. Ni-NTA agarose beads were collected in a Buchner funnel and washed with ~300 mL protein wash buffer (30 mM HEPES, pH 7.2, 150 mM NaCl, 20 mM imidazole). Beads were transferred to an Econo-Pak Chromatography column (Bio-Rad) and protein was eluted in 15 mL of elution buffer (30 mM HEPES, pH 7.2, 150 mM NaCl, and 200 mM imidazole). Proteins were concentrated using Amicon Ultracel 10 K filters (Millipore) and absorbance at 280 nm was measured using a Nanodrop 2000 spectrophotometer (Thermo Fisher Scientific) to determine protein concentration.

Surface plasmon resonance (SPR)

Experiments were performed using a Sierra SPR-32 Pro (Bruker). Ly6a-Fc fusion protein in HBS-P+ buffer (GE Healthcare) was immobilized to a protein A sensor chip at a capture level of ~1200−1500 response units (RUs). Twofold dilutions of rAAV beginning at 4×10^{12} vg mL^{-1} were injected at a flow rate of 10 μl min^{-1} with a contact time of 240 s and a dissociation time of 600 s. The protein A sensor chip was regenerated with 10 mM glycine pH 1.5 after each cycle. Kinetic data were double reference subtracted.

Bulk sequencing for capsid enrichment in ex vivo tissue

Ex vivo NHP or human brain slice cultures were either infected with the pool of viruses with an equivalent molar ratio or infected with PHP.eB packaging non-CAG-FXN-HA construct. After 7 or 10 days in vitro, the tissues were snap frozen and shipped to Caltech on dry ice. Tissues were immediately stored at −80 °C upon receipt. RNA was extracted from the whole tissue or half of the tissue following a slightly modified

Phenol/Chloroform protocol (Goertsen et al. 2021). RNA was further cleaned by treating with DNase using RNA Clean & Concentrator-5 kit (Zymo), and reverse transcription was done on up to 1 µg purified RNA using Superscript IV VILO Master Mix (Thermo Fisher). If DNA was needed from the tissue, DNA was extracted from the other half of the tissue using QIAamp DNA Mini Kit (Qiagen) following the manufacturer's instructions.

The barcoded FXN region was recovered from the resulting cDNA library or DNA using primers of 5′-TGGACCTAAGCGTTATGACTGGAC-3′ and 5′-GGAGCAACATAGTTAAGAATACCAGTCAATC-3′ and PCR was performed using Q5 2x Master Mix (New England BioLabs) at 25 cycles of 98 °C for 10 s, 63 °C for 15 s, and 72 °C for 20 s. Each sample was run in up to five reactions using up to 50 ng of cDNA or DNA, each, as a template. After PCR, samples were purified using DNA Clean & Concentrator-25 kit (Zymo). The barcoded FXN region was further recovered and the adapter sequence was added by performing PCR using primers of 5′-ACGCTCTTCCGATCTTGTTCCAGATTACGCTTGAG-3′ and 5′-TGTGCTCTTCCGATCTTGTAATCCAGAGGTTGATTATCG-3′ at ten cycles of 98 °C for 10 s, 55 °C for 15 s, and 72 °C for 20 s. Samples were then purified using DNA Clean & Concentrator-25 kit. Index sets in the NEBNext Dual Index Primers (New England BioLabs) were carefully chosen and added to the barcoded FXN region by performing PCR at ten cycles of 98 °C for 10 s, 60 °C for 15 s, and 72 °C for 20 s. To further separate the sequence for later next-generation sequencing (NGS), the PCR samples were run on a 2% low-melting-point agarose gel for separation and recovery of the 210 bp band.

NGS was performed on an Illumina MiSeq Next Generation Sequencer (Illumina) using a 150-cycle MiSeq Reagent Kit v3 (Illumina) following the manufacturer's procedure. All samples were pooled in an equal ratio to create a 4 nM library. 10% 20 pM PhiX control was spiked in to add diversity to the library. Demultiplexing was done by Base-Space Sequence Hub and the barcode counting analysis was performed using in-house Python code. For each brain slice culture, the enrichment of capsid variants was calculated by the ratio of the counts of their corresponding barcode to the counts of the corresponding barcode of the internal control capsid (e.g., AAV9 or PHP.eB). To correct any potential error due to titer determination, PCR amplification, or sequencing, DNA from the same pool of virus that was used for the brain slice culture infection was extracted, amplified, and included in the MiSeq NGS and analysis. The enrichment of the capsid variants was then normalized by the input viral DNA in the pool.

QPCR and RT-PCR for vector genomes and RNA transcripts in ex vivo tissue

We used quantitative PCR and quantitative RT-PCR to measure AAV variant transduction and expression in NHP slice cultures. We cut physiological slices (300-microns thick) from the superior temporal gyrus of one adult (age 14 years and 1 month, weight 10.83 kg) *M. mulatta* animal housed at the University of Washington National Primate facility. The animal had been planned for routine euthanasia and we collected the brain as part of the facility's tissue distribution program. We sectioned a block of superior temporal gyrus and the slices were recovered as described previously[53], and then we cultured the slices on the air-liquid membrane interface. At 30 min following slice plating, we transduced the slices on their face with ~1−2 µL CAG-EGFP vectors, packaged in AAV9 or X1.1 (titers approximately 5e13 vg/mL). We performed transductions on three biological replicates for each vector. We refreshed the culture medium every 48 h until tissue harvest at 8 days in vitro. At harvest, we imaged the slices to confirm transduction, and then bisected the slices, and quick-froze each slice half in a dry ice-ethanol bath, then stored them at −20° C until nucleic acid processing.

One slice half (~20 mg wet tissue weight) was processed to isolate DNA, and the other slice half was processed to isolate RNA for cDNA preparation. We isolated DNA using the Qiagen DNeasy Blood and Tissue Kit (Qiagen, catalog # 69504) with no modifications to the protocol, yielding ~3–5 ug total DNA per slice half. We isolated RNA using first TRIzol (Thermo Fisher Scientific, catalog #15596026) to isolate crude dilute RNA, which we then purified and concentrated using the PureLink RNA Mini Kit (Thermo Fisher Scientific, catalog # 12183018 A). On the column of the PureLink RNA Mini Kit, we also performed DNA digestion by modifying the first wash as follows: we first washed with 350 uL of Wash Buffer 1, then added 80 uL of RNase-Free DNaseI in RDD buffer (Qiagen catalog # 79254) and incubated the column at room temperature for 15 min, then washed again with 350 uL of Wash Buffer 1, and proceeded with washing and elution as per the protocol. Typically, this technique yielded ~1.5 ug DNA-free total RNA per slice half. We then performed first-strand cDNA synthesis from 400 ng total RNA in 20 uL reactions using Promega GoScript Reverse Transcription Kit (Promega, catalog # A5000).

For quantitative PCR, we used 100 ng DNA in a 20 uL amplification reaction using the following Taqman probes (all from Thermo Fisher Scientific): EGFP-FAM probe (Assay ID Mr04097229_mr, catalog #4331182), and custom genomic reference probe CN2386-2-VIC (Assay ID ARH6DUK catalog #4448512, designed to target both *M. mulatta* and *M. nemestrina*). For quantitative RT-PCR, we used 1 uL of cDNA (20 ng of original total RNA) in a 10 uL amplification reaction using the following probes: EGFP-FAM probe (same probe as used for DNA detection) and custom housekeeping reference probe GAPDH-VIC (Assay ID APAAHJR, catalog #4448508, designed to target both *M. mulatta* and *M. nemestrina*). We amplified and detected these reactions on a Roche Lightcycler II instrument alongside standard curves consisting of serial dilutions of plasmid DNA or purified PCR amplicons in the case of GAPDH. Then we extracted Cp values using the second derivative method, calculated the relative abundances of vector DNA/RNA with respect to internal reference probes, and normalized these ratios to those observed with the AAV9 vector. In some cases, the EGFP-FAM probe was so abundant that it interfered with the detection of the VIC reference probes; in these cases, the reactions were run in separate wells.

Data analysis

1. Quantification of AAV transduction in vivo. The quantification of AAV transduction across tissues was carried out by manually counting fluorescent expression resulting from the AAV genome. ImageJ was used for this purpose.

2. NGS data alignment, processing, and analysis. The NGS data analysis was carried out using a custom data-processing pipeline with scripts written in Python[13] (https://github.com/GradinaruLab/mCREATE) and using plotting software such as Plotly, Seaborn, and GraphPad PRISM 7.05. The AAV9 capsid structure model was produced with PyMOL.

3. Enrichment score calculation. The enrichment score for a variant was determined using the following formula:

Enrichment score of variant "x" in tissue1 = log10 [(Enrichment of variant "x" in tissue1)/(Enrichment of variant "x" in the virus pool)]

Enrichment of variant "x" in tissue1 = (Variant "x" RC in tissue library)/(Sum of variants N RC in tissue1)

Enrichment of variant "x" in the virus pool = (Variant "x" RC in virus pool)/(Sum of variants N RC in virus pool)

Where N is the total number of variants in a library.

4. Fold change calculation. The fold change of a variant "x" to AAV9 = (The enrichment score of "x")/(The enrichment score of AAV9).

Statistics and reproducibility

The numbers of mice used in each experiment are indicated in figure legends. No data were excluded from the analyses. Statistical

significance was calculated as described in figure legends. Statistical analysis was performed with GraphPad Prism 9.0.1 software.

Reporting summary

Further information on research design is available in the Nature Portfolio Reporting Summary linked to this article.

Data availability

All sequences of AAV variants developed in this study are provided in materials and methods. Key vector plasmid AAV-X1.1 is available at Addgene (#196836) and also at the Beckman Institute CLOVER Center (https://clover.caltech.edu/). Source data are provided with this paper. Other data that support the findings of this study are available from the corresponding author upon request.

Code availability

The code used for M-CREATE data analysis were published previously[13] and are available on GitHub: https://github.com/GradinaruLab/mCREATE.

References

1. Yu, X., Ji, C. & Shao, A. Neurovascular unit dysfunction and neuro-degenerative disorders. *Front. Neurosci.* **14**, 334 (2020).
2. Xiao, M., Xiao, Z., Yang, B., Lan, Z. & Fang, F. Blood-brain barrier: more contributor to disruption of central nervous system home-ostasis than victim in neurological disorders. *Front. Neurosci.* **14**, 764 (2020).
3. Profaci, C. P., Munji, R. N., Pulido, R. S. & Daneman, R. The blood-brain barrier in health and disease: important unanswered ques-tions. *J. Exp. Med.* **217**, e20190062 (2020).
4. Yang, A. C. et al. A human brain vascular atlas reveals diverse mediators of Alzheimer's risk. *Nature* **603**, 885–892 (2022).
5. Aschauer, D. F., Kreuz, S. & Rumpel, S. Analysis of transduction efficiency, tropism and axonal transport of AAV serotypes 1, 2, 5, 6, 8 and 9 in the mouse brain. *PLoS ONE* **8**, e76310 (2013).
6. Watakabe, A. et al. Comparative analyses of adeno-associated viral vector serotypes 1, 2, 5, 8 and 9 in marmoset, mouse and macaque cerebral cortex. *Neurosci. Res.* **93**, 144–157 (2015).
7. Deverman, B. E. et al. Cre-dependent selection yields AAV variants for widespread gene transfer to the adult brain. *Nat. Biotechnol.* **34**, 204–209 (2016).
8. Deverman, B. E., Ravina, B. M., Bankiewicz, K. S., Paul, S. M. & Sah, D. W. Gene therapy for neurological disorders: progress and pro-spects. *Nat. Rev. Drug Discov.* **17**, 641–659 (2018).
9. Hudry, E. & Vandenberghe, L. H. Therapeutic AAV gene transfer to the nervous system: a clinical reality. *Neuron* **101**, 839–862 (2019).
10. Chen, X. et al. Engineered AAVs for non-invasive functional trans-gene expression in rodent and non-human primate central and peripheral nervous systems. *Neuron* **110**, 2242–2257 (2022).
11. Challis, R. C. et al. Adeno-associated virus toolkit to target diverse brain cells. *Ann. Rev. Neurosci.* **45**, 447–469 (2022).
12. Chan, K. Y. et al. Engineered AAVs for efficient noninvasive gene delivery to the central and peripheral nervous systems. *Nat. Neu-rosci.* **20**, 1172–1179 (2017).
13. Ravindra Kumar, S. et al. Multiplexed Cre-dependent selection yields systemic AAVs for targeting distinct brain cell types. *Nat. Methods* **17**, 541–550 (2020).
14. Goertsen, D. et al. AAV capsid variants with brain-wide transgene expression and decreased liver targeting after intravenous delivery in mouse and marmoset. *Nat. Neurosci.* **25**, 106–115 (2021).
15. Körbelin, J. et al. A brain microvasculature endothelial cell-specific viral vector with the potential to treat neurovascular and neurolo-gical diseases. *EMBO Mol. Med.* **8**, 609–625 (2016).
16. Sundaram, S. M. et al. Gene therapy targeting the blood-brain barrier improves neurological symptoms in a model of genetic MCT8 deficiency. *Brain* **145**, 4262–4274.
17. Greig, J. A. et al. Loss of transgene expression limits liver gene therapy in primates. Preprint at *bioRxiv* https://doi.org/10.1101/2022.03.24.485675 (2022).
18. Hamilton, B. A. & Wright, J. F. Challenges posed by immune responses to AAV vectors: addressing root causes. *Front. Immunol.* https://www.frontiersin.org/article/10.3389/fimmu.2021.675897 (2021).
19. Bočkor, L. et al. Repeated AAV-mediated gene transfer by serotype switching enables long-lasting therapeutic levels of HUgt1a1 enzyme in a mouse model of Crigler–Najjar syndrome type I. *Gene Ther.* **24**, 649–660 (2017).
20. Colella, P., Ronzitti, G. & Mingozzi, F. Emerging issues in AAV-mediated in vivo gene therapy. *Mol. Ther. Methods Clin. Dev.* **8**, 87–104 (2018).
21. Lykken, E. A., Shyng, C., Edwards, R. J., Rozenberg, A. & Gray, S. J. Recent progress and considerations for AAV gene therapies tar-geting the central nervous system. *J. Neurodev. Disord.* **10**, 16 (2018).
22. Wang, D., Tai, P. W. & Gao, G. Adeno-associated virus vector as a platform for gene therapy delivery. *Nat. Rev. Drug Discov.* **18**, 358–378 (2019).
23. Sawamoto, K., Chen, H., Alméciga-Díaz, C. J., Mason, R. W. & Tomatsu, S. Gene therapy for mucopolysaccharidoses. *Mol. Genet. Metab.* **123**, 59–68 (2018).
24. Ponder, K. P. & Haskins, M. E. Gene therapy for mucopolysacchar-idosis. *Expert Opin. Biol. Ther.* **7**, 1333–1345 (2007).
25. Zapolnik, P. & Pyrkosz, A. Gene therapy for mucopolysaccharidosis type II—A review of the current possibilities. *Int. J. Mol. Sci.* **22**, 5490 (2021).
26. Kucukdereli, H. et al. Control of excitatory CNS synaptogenesis by astrocyte-secreted proteins Hevin and SPARC. *Proc. Natl Acad. Sci. USA* **108**, E440–E449 (2011).
27. Risher, W. C. et al. Astrocytes refine cortical connectivity at den-dritic spines. *ELife* https://doi.org/10.7554/eLife.04047 (2014).
28. Singh, S. K. et al. Astrocytes assemble thalamocortical synapses by bridging Nrx1α and NL1 via Hevin. *Cell* **164**, 183–196 (2016).
29. Geisler, A. & Fechner, H. MicroRNA-regulated viral vectors for gene therapy. *World J. Exp. Med.* **6**, 37–54 (2016).
30. Isakova, A., Fehlmann, T., Keller, A. & Quake, S. R. A mouse tissue atlas of small noncoding RNA. *Proc. Natl Acad. Sci. USA* **117**, 25634–25645 (2020).
31. Geisler, A. et al. MicroRNA122-regulated transgene expression increases specificity of cardiac gene transfer upon intravenous delivery of AAV9 vectors. *Gene Ther.* **18**, 199–209 (2011).
32. DiMattia, M. A. et al. Structural insight into the unique properties of adeno-associated virus serotype 9. *J. Virol.* **86**, 6947–6958 (2012).
33. Pulicherla, N. et al. Engineering liver-detargeted AAV9 vectors for cardiac and musculoskeletal gene transfer. *Mol. Ther.* **19**, 1070–1078 (2011).
34. Shen, S. et al. Glycan binding avidity determines the systemic fate of adeno-associated virus type 9. *J. Virol.* **86**, 10408–10417 (2012).
35. Bell, C. L., Gurda, B. L., Vliet, K. V., Agbandje-McKenna, M. & Wil-son, J. M. Identification of the galactose binding domain of the adeno-associated virus serotype 9 capsid. *J. Virol.* **86**, 7326–7333 (2012).
36. Adachi, K., Enoki, T., Kawano, Y., Veraz, M. & Nakai, H. Drawing a high-resolution functional map of adeno-associated virus capsid by massively parallel sequencing. *Nat. Commun.* **5**, 3075 (2014).
37. Zhang, R. et al. Adeno-associated virus 2 bound to its cellular receptor AAVR. *Nat. Microbiol.* **4**, 675–682 (2019).

38. Hordeaux, J. et al. The GPI-linked protein LY6A drives AAV-PHP.B transport across the blood-brain barrier. *Mol. Ther.* **27**, 912–921 (2019).

39. Huang, Q. et al. Delivering genes across the blood-brain barrier: LY6A, a novel cellular receptor for AAV-PHP.B capsids. *PLoS ONE* **14**, e0225206 (2019).

40. Batista, A. R. et al. Ly6a differential expression in blood-brain barrier is responsible for strain specific central nervous system transduction profile of AAV-PHP.B. *Hum. Gene Ther.* **31**, 90–102 (2020).

41. Armulik, A. et al. Pericytes regulate the blood-brain barrier. *Nature* **468**, 557–561 (2010).

42. Mäe, M. A. et al. Single-cell analysis of blood-brain barrier response to pericyte loss. *Circ. Res.* **128**, e46–e62 (2021).

43. Bortolussi, G. et al. Life-long correction of hyperbilirubinemia with a neonatal liver-specific AAV-mediated gene transfer in a lethal mouse model of Crigler–Najjar syndrome. *Hum. Gene Ther.* **25**, 844–855 (2014).

44. Tan, F. et al. AAV-Ie enables safe and efficient gene transfer to inner ear cells. *Nat. Commun.* **10**, 3733 (2019).

45. Lau, C., Ho, J. W., Lo, P. W. & Tin, C. Targeted transgene activation in the brain tissue by systemic delivery of engineered AAV1 expressing CRISPRa. *Mol. Ther. Nucleic Acids* **16**, 637–649 (2019).

46. Martino, R. A. et al. Context-specific function of the engineered peptide domain of PHP.B. *J. Virol.* **95**, e0116421 (2021).

47. Pietersz, K. et al. PhP.B enhanced adeno-associated virus mediated-expression following systemic delivery or direct brain administration. *Front. Bioeng. Biotechnol.* **9**, 679483 (2021).

48. Lloyd-Burton, S. & Roskams, A. J. SPARC-like 1 (SC1) is a diversely expressed and developmentally regulated matricellular protein that does not compensate for the absence of SPARC in the CNS. *J. Comp. Neurol.* **520**, 2575–2590 (2012).

49. Mongrédien, R. et al. Cartography of hevin-expressing cells in the adult brain reveals prominent expression in astrocytes and parvalbumin neurons. *Brain Struct. Funct.* **224**, 1219–1244 (2019).

50. Kähler, A. K. et al. Association analysis of schizophrenia on 18 genes involved in neuronal migration: MDGA1 as a new susceptibility gene. *Am. J. Med. Genet. B Neuropsychiatr. Genet.* **147B**, 1089–1100 (2008).

51. Zhurov, V. et al. Molecular pathway reconstruction and analysis of disturbed gene expression in depressed individuals who died by suicide. *PLoS ONE* **7**, e47581 (2012).

52. De Rubeis, S. et al. Synaptic, transcriptional and chromatin genes disrupted in autism. *Nature* **515**, 209–215 (2014).

53. Ting, J. T. et al. A robust ex vivo experimental platform for molecular-genetic dissection of adult human neocortical cell types and circuits. *Sci. Rep.* **8**, 8407 (2018).

54. Rivière, C., Danos, O. & Douar, A. M. Long-term expression and repeated administration of AAV type 1, 2 and 5 vectors in skeletal muscle of immunocompetent adult mice. *Gene Ther.* **13**, 1300–1308 (2006).

55. Majowicz, A. et al. Successful repeated hepatic gene delivery in mice and non-human primates achieved by sequential administration of AAV5ch and AAV1. *Mol. Ther.* **25**, 1831–1842 (2017).

56. Stanimirovic, D. B., Sandhu, J. K. & Costain, W. J. Emerging technologies for delivery of biotherapeutics and gene therapy across the blood-brain barrier. *BioDrugs* **32**, 547–559 (2018).

57. Terstappen, G. C., Meyer, A. H., Bell, R. D. & Zhang, W. Strategies for delivering therapeutics across the blood-brain barrier. *Nat. Rev. Drug Discov.* **20**, 362–383 (2021).

58. Matsuzaki, Y. et al. Intravenous administration of the adeno-associated virus-PHP.B capsid fails to upregulate transduction efficiency in the marmoset brain. *Neurosci. Lett.* **665**, 182–188 (2018).

59. Krolak, T. et al. A high-efficiency AAV for endothelial cell transduction throughout the central nervous system. *Nat. Cardiovasc. Res.* **1**, 389–400 (2022). no. 4 (2022).

60. Jennings, C. G. et al. Opportunities and challenges in modeling human brain disorders in transgenic primates. *Nat. Neurosci.* **19**, 1123–1130 (2016).

61. Bey, K. et al. Intra-CSF AAV9 and AAVrh10 administration in non-human primates: promising routes and vectors for which neurological diseases? *Mol. Ther. Methods Clin Dev* **17**, 771–784 (2020).

62. Challis, R. et al. Systemic AAV vectors for widespread and targeted gene delivery in rodents. *Nat. Protoc.* **14**, 379 (2019).

63. Lindblom, P. et al. Endothelial PDGF-B retention is required for proper investment of pericytes in the microvessel wall. *Genes Dev.* **17**, 1835–1840 (2003).

64. Yardeni, T., Eckhaus, M., Morris, H. D., Huizing, M. & Hoogstraten-Miller, S. Retro-orbital injections in mice. *Lab Anim.* **40**, 155–160 (2011).

65. Berg, J. et al. Human neocortical expansion involves glutamatergic neuron diversification. *Nature* **598**, 151–158 (2021).

66. Ting, J. T., Daigle, T. L., Chen, Q. & Feng, G. Acute brain slice methods for adult and aging animals: application of targeted patch clamp analysis and optogenetics. *Methods Mol. Biol.* **1183**, 221–242 (2014).

67. Mayerich, D., Abbott, L. & McCormick, B. Knife-edge scanning microscopy for imaging and reconstruction of three-dimensional anatomical structures of the mouse brain. *J. Microsc.* **231**, 134–143 (2008). Pt 1.

68. Ragan, T. et al. "Serial two-photon tomography for automated ex vivo mouse brain imaging. *Nat Methods* https://doi.org/10.1038/nmeth.1854. (2012).

69. Campbell, R. SainsburyWellcomeCentre/BakingTray: Jan 2020. *Zenodo.* https://doi.org/10.5281/zenodo.3631610 (2020).

70. Campbell, R. et al. SainsburyWellcomeCentre/StitchIt: last release of stitching model 1. *Zenodo.* https://doi.org/10.5281/zenodo.3941901 (2020).

71. Ippolito, D. M. & Eroglu, C. Quantifying synapses: an immunocytochemistry-based assay to quantify synapse number. *J. Vis. Exp.* **45**, 2270 (2010).

Acknowledgements

Author contributions

X.C. and V.G. designed the experiments. X.C., D.A.W., J. T.T., M. Z., D.S.B., H.S., S.R.K., T.F.S., E.E.S., D.G., V.N. performed experiments. D.A.W. assisted with the characterization of the vectors across models. D.S.B. and C.E. designed and conducted the in vivo Hevin expression experiments. J.T.T., M.Z., D.G., V.O., N.T., N.W., J.M., Y.B., D.M., B.G., B.P.L., and E.S.L assisted with the characterization of variants in ex vivo macaque and human brain slices. T.M. and E.S. assisted with the SPR experiment and the Ly6a experiment in HEK293T cells. S.H. and A.K. assisted with the characterization of the vectors in pericyte-deficient mice and vascular cell type-specific transduction. S.R.K. assisted with the HBMEC experiment and early iteration of the library. C.M.A. assisted with tissue processing in the macaque. X.D. generated the AAV1 and AAV9 models. V.P. and A.A. assisted with the characterization in rat with the support of the staff at SWC. V.N. and C.T.M. assisted with the characterization of the virus in marmoset with the support of vet staff at UCSD. L.J.C. and A.F. assisted with the characterization of the virus in rhesus macaque with the support of vet staff at UC Davis. X.C. prepared the figures with input from all authors. X.C. and V.G. wrote the manuscript with input from all authors. V.G. supervised all aspects of the work.

Competing interests

The California Institute of Technology has one patent pending for the sequences described in this manuscript, with X.C. and V.G. listed as inventors (PCT Patent Application No: PCT/US2022/027516). V.G. is a co-founder and board member of Capsida Biotherapeutics, a fully integrated AAV engineering and gene therapy company. The remaining authors declare no competing interests.

Additional information

Supplementary information The online version contains supplementary material available at https://doi.org/10.1038/s41467-023-38582-7.

Correspondence and requests for materials should be addressed to Viviana Gradinaru.

Peer review information *Nature Communications* thanks the anonymous reviewers for their contribution to the peer review of this work. A peer review file is available.

Reprints and permissions information is available at http://www.nature.com/reprints

Publisher's note Springer Nature remains neutral with regard to jurisdictional claims in published maps and institutional affiliations.

[1]Division of Biology and Biological Engineering, California Institute of Technology, Pasadena, CA 91125, USA. [2]Department of Cell Biology, Duke University Medical Center, Durham, NC 27710, USA. [3]Allen Institute for Brain Science, Seattle, WA, USA. [4]Department of Neurosurgery, Clinical Neuroscience Center, Zürich University Hospital, University of Zürich, Zürich, Switzerland. [5]Sainsbury Wellcome Centre, University College London, London, UK. [6]Department of Psychology and California National Primate Research Center, University of California, Davis, Davis, CA 95616, USA. [7]Cortical Systems and Behavior Lab, University of California San Diego, La Jolla, CA 92039, USA. [8]Neuroscience Center Zürich, University of Zürich and ETH Zürich, Zürich, Switzerland. [9]Department of Physiology and Biophysics, University of Washington, Seattle, WA, USA. ✉e-mail: viviana@caltech.edu